HHS Public Access

Author manuscript

Adv Drug Deliv Rev. Author manuscript; available in PMC 2021 March 23.

Published in final edited form as:

Adv Drug Deliv Rev. 2020 January 01; 153: 147–168. doi:10.1016/j.addr.2020.03.003.

Imaging and quantifying drug delivery in skin – Part 2: fluorescence and vibrational spectroscopic imaging methods

Ana-Maria Pena[a], **Xueqin Chen**[a], **Isaac Pence**[b], **Thomas Bomschlögl**[a], **Sinyoung Jeong**[b], **Sébastien Grégoire**[1,a], **Gustavo S. Luengo**[a], **Philippe Hallegot**[a], **Peyman Obeidy**[b], **Amin Feizpour**[b], **Kin F. Chan**[c], **Conor L. Evans**[1,b]

[a]L'Oréal Research and Innovation, 1 avenue Eugène Schueller BP22, 93600 Aulnay-sous-Bois, France

[b]Wellman Center for Photomedicine, Massachusetts General Hospital, Harvard Medical School, CNY149-3, 13th St, Charlestown, MA 02129

[c]Simpson Interventions, Inc., Woodside, CA 94062

Abstract

Understanding the delivery and diffusion of topically-applied drugs on human skin is of paramount importance in both pharmaceutical and cosmetics research. This information is critical in early stages of drug development and allows the identification of the most promising ingredients delivered at optimal concentrations to their target skin compartment. Different skin imaging methods, invasive and non-invasive, are available to characterize and quantify the spatiotemporal distribution of a drug within *ex vivo* and *in vivo* human skin. The first part of this review detailed invasive imaging methods (autoradiography, MALDI and SIMS). This second part reviews non-invasive imaging methods that can be applied *in vivo*: i) fluorescence (conventional, confocal, multiphoton) and second harmonic generation microscopies and ii) vibrational spectroscopic imaging methods (infrared, confocal Raman, coherent Raman scattering microscopies). Finally, a decision-maker flow chart of imaging methods is presented to guide human skin *ex vivo* and *in vivo* drug delivery studies.

Keywords

Human skin; drug delivery; fluorescence; confocal; multiphoton; 2PEF; SHG; FLIM; IR; Raman; CARS; SRS

1. Introduction

In the first part of this review, we introduced mass spectrometry and autoradiographic tools that can be used for tracking and quantification of drugs and compounds within skin [1].

[1]**Corresponding Authors**: Sébastien Grégoire, sebastien.gregoire@rd.loreal.com; Conor L. Evans, evans.conor@mgh.harvard.edu.

These sensitive methods are capable of analyzing skin samples but are largely restricted to use in *ex vivo* samples. Optical imaging approaches can offer substantial benefits for the study of drug and compound uptake within skin, such as the ability to quantitatively visualize the spatiotemporal dynamics of molecular flow and flux in tissue. As these tools are non-invasive and non-destructive, many optical imaging methods can be used to repeatedly image and collect three-dimensional chemical tomograms of the same sample region or individual over time. However, the light-based tools have inherent limits due to the limited penetration depth of light, but their potential for translation to human use makes them exciting approaches for examining pharmacokinetics (PK) in subjects and patients. In this second part of the review, we introduce and discuss i) fluorescence (conventional, confocal, multiphoton) and second harmonic generation microscopies) and ii) vibrational spectroscopic imaging methods (infrared, confocal Raman, coherent Raman scattering microscopies) available for imaging and quantifying molecular species in human skin.

The goal of this review is not to give a full literature review of every optical application in the study of drug delivery in human skin, but rather to acquaint the reader with the principle of each imaging technique and how these technologies are being used to advance the knowledge in this field of human skin drug delivery.

2. Fluorescence (1PEF, 2PEF, FLIM) and second harmonic generation microscopies (SHG)

The skin distribution profile of a cosmetic or pharmaceutically active ingredient (API) with natural fluorescence [2] properties can be assessed using fluorescence-based microscopies. Most of the studies in this field are conducted on cell cultures and *ex vivo* human skin samples using conventional and confocal fluorescence microscopies. In the past twenty years, the advent of multiphoton technologies opened the door to the non-invasive assessment of a fluorescent ingredient distribution *in vivo* in human skin clinical trials [3-7]. For fluorophores that share significant spectral overlap, it is also possible to use fluorescence lifetime imaging microscopy (FLIM) to discriminate exogenous fluorescent ingredients from the endogenous, natural fluorophores of human skin, provided that their fluorescence lifetime properties are different. Moreover, cosmetic ingredients and APIs that have non-linear optical properties at the macromolecular scale, such as the second harmonic generation, can also be detected *in vivo* using multiphoton SHG imaging [8] [9, 10].

Fluorescence-based imaging of different exogenous fluorophores, used as model drugs, has also found applications in the development of transdermal drug delivery systems. These technologies [11, 12] aim at enhancing the penetration of an ingredient into the skin, across the skin's barrier layer, the *stratum corneum*. These technologies span from first-generation (patches), second-generation (chemical enhancers, noncavitational ultrasound, iontophoresis) up to third-generation delivery systems targeting the *stratum corneum* using methods such as microneedles, thermal ablation (radiofrequency, fractional laser), microdermabrasion, electroporation, photoacoustic mediation [13] and cavitational ultrasound.

2.1. Conventional fluorescence microscopy

Conventional and confocal fluorescence microscopies [14] are based on the phenomenon of linear one-photon excitation. One-photon excited fluorescence (1PEF) signals are emitted by a fluorescent molecule that has reached the excited state by absorption of a single photon. The return to the ground state occurs rapidly, typically within a few nanoseconds, through the emission of a fluorescence photon. Fluorescence typically occurs from molecules containing aromatic structures that are excited in the ultraviolet (UV), visible (VIS), and near-infrared (NIR) wavelength range. In terms of spectral properties, the fluorescence emission is “Stokes” shifted, due to intramolecular vibrational relaxation processes, and is therefore emitted at longer wavelengths compared to the excitation wavelength.

In conventional wide-field fluorescence microscopy [15], a parallel beam of light, from an arc-discharge lamp or LED light source, is spectrally filtered by an excitation filter and used to illuminate the sample under the microscope’s objective. The fluorescence light is collected in the backwards (epi) direction, separated from the excitation light using dichroic mirrors and optical filters and detected on a camera. This type of fluorescence imaging works best with thin samples such as cellular monolayers or histological sections with a thickness of about 10 μm and image resolution can be enhanced through deconvolution.

When imaging thicker samples, the fluorescence signals arising from the tissues above and below the focal plane will contribute out-of-focus light to the collected image, resulting in a blurred picture. One can use conventional fluorescence microscopy to map the distribution of fluorescent ingredients within thin human skin histological sections. Fluorescence imaging can be accompanied by transmitted light imaging for morphological identification of the *stratum corneum*, living epidermis and dermal layers.

Using transmitted light microscopy along with both conventional fluorescence and FLIM (fluorescence lifetime imaging; see section 2.4 for FLIM description), Frombach *et al.* investigated the potential of core-multishell nanocarriers (CMS-NC) for drug delivery across the skin barrier [16]. CMS-NC are able to solubilize a multitude of hydrophobic drugs in hydrophilic media and vice versa while exhibiting a high release rate. The authors characterized the CMS-NC’s distribution and the penetration and release of dexamethasone (DXM), in excised full-thickness human skin focusing on the role of hair follicles. Figure 1A and B show conventional fluorescence images of both the carrier and the drug’s distribution within the skin after topical application of DXM-CMS-NC on intact *ex vivo* human skin. The images were acquired on thin histological sections and reveal the drug accumulation in skin furrows and around hair follicles.

Moreover, the authors found that small amounts of the nanocarrier translocated into the living epidermis, appearing as punctate spots. In order to verily that the observed fluorescence indeed originated from ICC-CMS-NC (indocarbocyanine-labelled CMS-NC) and not from endogenous autofluorescence, the skin sections were characterized by conventional FLIM and transmitted light images (see Figure 1C, D, E). The authors not only detected the fluorescence intensity, but also measured the fluorescence lifetime i.e. the ensemble average time between the fluorophore’s excitation and its return to the ground state. Fluorophores with similar emission spectra can be differentiated by FLIM provided

they display different fluorescence lifetimes. Figure IE shows examples of fluorescence decay traces of skin autofluorescence (green) and ICC-CMS-NC (cyan, red). FLIM data can be analyzed in different ways: by fitting the fluorescence decay trace with multiple exponential decay functions, by phasor analysis or by pattern analysis. The first two methods are briefly described in section 2.4. In the above example, the authors used the pattern analysis to identify the pixels with similar fluorescence decay traces [17]. The analysis revealed three distinct fluorescence lifetime signatures (Figure IE): in the *stratum corneum* and within the hair follicle, the slow fluorescence decay signature (cyan) of ICC-CMS-NC was observed, while a fast fluorescence decay signature (red) was found in the center of hair follicles and occasionally in small spots in the viable epidermis and dermis.

The above example highlights one challenge routinely encountered when using fluorescence microscopy: the presence of autofluorescence from endogenous fluorescent compounds. Indeed, skin contains many natural fluorescence molecules, such as collagen, elastin, nicotinamide adenine dinucleotide (NADH), and flavin adenine dinucleotide (FAD) as well as porphyrin molecules synthesized by bacterial in the skin microbiome [18, 19]. These endogenous fluorophores can provide important information as to the composition and state of the skin [20-22], but also can emit at the same wavelength as compounds of interest [23]. Skin autofluorescence can also be highly heterogeneous from person to person. In a recent study examining facial skin samples, a six-fold difference in total autofluorescence intensity was observed across more than forty subjects, showcasing a challenge in quantitatively measuring fluorescent drug uptake in skin [24]. More problematically, the skin structures that give rise to autofluorescence are themselves heterogenous: individual structures, such as sebaceous glands, have non-identical levels of autofluorescence, and the structures themselves are heterogeneously spatially distributed within skin [23]. This degree of subject and spatial heterogeneity has motivated the need to study larger numbers of skin specimens with advanced forms of fluorescence microscopy.

2.2. Confocal fluorescence microscopy

Confocal fluorescence microscopy [14] serves an important role in bridging the gap between thin, two dimensional samples such as tissue sections and three-dimensional samples such as *ex vivo* human skin biopsies. After topical application of a fluorescent compound onto the skin, a biopsy can be taken and analyzed either in 2D with histology or in 3D with confocal fluorescence via fresh or whole-mount methods. Confocal fluorescence microscopy enables three-dimensional spatial imaging of the distribution of a fluorescent compound within human skin up to a depth of about 50-70 μm, depending on the concentration, emission wavelength, and fluorescent quantum yield of the fluorescent compound as well as the absorption and diffusion properties of the skin. Compared to conventional fluorescence microscopy, the whole sample volume is not continuously illuminated but instead raster scanned with a laser beam focused in the tissue by an objective lens. The fluorescence light is epi-collected, de-scanned, separated from the laser light with a dichroic beam splitter and collected by detectors. The image formation is derived only from the focal plane and not from out-of-focus planes as in wide-field microscopy via the use of a spatial filter in the de-scanned beam path. Spatial filters, known as “confocal pinholes” in this context, are placed conjugate to the microscope focal plane such that only fluorescence signal arising from the

focal point can efficiently pass through the aperture. A 2D image can be acquired by raster scanning the laser light in *x* and *y* directions; a 3D volume is constructed by acquiring a "stack" of individual 2D planes along the microscope axial ("z") direction by either moving the objective lens or the sample itself. The use of the confocal pinhole allows for so-called "optical sectioning". Confocal fluorescence microscopy offers an improved image contrast over conventional fluorescence imaging due to the elimination of out-of-focus fluorescence and an improved lateral (~200-400 nm) and axial (~0,4-1 μm) resolutions. The practical imaging resolutions depend on the fluorophore emission wavelength, numerical aperture of the objective and index of refraction of the sample.

Limón et al. used confocal fluorescence microscopy to study the cellular internalization of serine protease inhibitor-coated water-soluble gold nanoparticles as a novel targeted approach for the treatment of inflammatory skin diseases [25]. Figure 2A shows the distribution of BODIPY-labeled gold nanoparticles inside the cytoplasm of human keratinocytes. Using the same imaging technique, Holmes *et al.* studied the intracellular labile zinc uptake within keratinocytes after application of zinc pyrithione (ZnPT), an active component incorporated in an extensive range of topically applied commercial products used, for example, in the management of dandruff (see Figure 2B) [8]. The authors used an exogenous fluorophore, ZinPyr-1, to highlight the endogenous levels of intracellular labile zinc in control cells and in cells treated with increasing concentrations of ZnPT. Instead of using cellular membrane staining, the authors overlaid the confocal fluorescence images with bright field images to map the fluorophore's distribution within the cells.

The 3D distribution of a fluorophore within a skin sample can be characterized with this imaging technique as demonstrated by Yamada *et al.* for the *ex vivo* study of elongated microparticles (EMP) combined with tailorable nanoemulsions (P20TNE) to enhance topical delivery of hydrophobic drug surrogates in human skin [3]. As a hydrophobic drug surrogate, they used a fluorescent lipophilic dye DiI, incorporated within P20TNE, and characterized its distribution through the epidermis on freshly excised human skin (see Figure 3 left). The confocal fluorescence images of EMP+P20TNE alginate group show a detectable signal of DiI around the dermal-epidermal junction and demonstrate that topical delivery of TNE was enhanced by EMP and alginate.

In vivo confocal fluorescence imaging of a fluorescent compound topically applied to living human skin suffers from strong UV / VIS laser light attenuation by tissue constituents (mainly melanin and hemoglobin), which can limit imaging depth. Still, a remarkable amount of information can be gleaned from drug penetration through the epidermis and the upper layers of the dermis. As reviewed by Alvarez-Roman, confocal fluorescence imaging can follow and quantify the penetration of a wide range of fluorescent compounds and nanoparticles within skin tissue [26]. It should be noted that confocal fluorescence methods can cause rather significant photobleaching of fluorescence compounds, as all fluorophores along the optical axis are excited. This can also lead to photodamage of the skin tissues, as the excited fluorophores can generate reactive radical species [27].

Confocal fluorescence imaging in the skin is often accompanied by confocal reflectance imaging, which can be used to acquire 3D structural images of skin tissue [28-31]. In this

imaging mode, the excitation and detection wavelengths are set to be identical; the laser light reflected and/or scattered by the sample is passed through the confocal pinhole and detected to provide contrast that arises from refractive index changes in the sample. A 3D skin image in confocal reflection microscopy facilitates identification of the *stratum corneum*, living epidermis, dermis layers, and even the flow of blood through skin capillary loops [30]. Confocal reflection microscopy can use any wavelength of light, but is typically carried out *in vivo* using red or near-infrared lasers to achieve the highest possible penetration depth within tissue. Figure 3 (middle) shows an example of confocal reflectance images of *ex vivo* living abdominal skin treated with elongated microparticles combined with tailorable nanoemulsions and alginate. The reflectance images allow for the easy discrimination of elongated microparticles from the cells to assessing their penetration in the upper dermis.

2.3. Multiphoton – 2PEF, SHG contrast modes

Multiphoton microscopy opens up the ability to image fluorescent molecules deep within *in vivo* human skin and has many applications in applied cosmetic and pharmaceutical research. Multiphoton imaging has been used in studies spanning from the characterization of human skin pigmentation, age-related or photo-aging changes [32-41], and dermatological disorders [42-55] to the assessment of pharmaceutical and cosmetic products penetration in human skin [3, 4, 8, 25, 40, 55-63]. Using multiphoton imaging, fluorescent compounds and skin structural components can be characterized at sub-micrometer (~400 nm lateral and ~2 μm axial) resolutions within the epidermis and superficial dermis up to a depth of ~200 μm [64]. In addition to visualizing specific drugs of interest, multiphoton imaging can be leveraged to visualize specific intrinsic emission profiles associated with cellular and extracellular matrix skin constituents such as keratin, NADH, FAD, melanin, and elastin. In addition, so-called “harmonic” generation microscopy methods can be used to visualize the microstructure of tissue, including specific types of fibrillar collagens [65-72]. Discrimination of exogenous fluorescent compounds from the endogenous tissue fluorescence is possible when the compound of interest has fluorescence properties (intensity, emission spectrum, lifetime) that differ appreciably from those of skin constituents.

Multiphoton fluorescence and harmonic microscopies make use of ultrashort pulsed near-infrared or infrared lasers. In multiphoton processes, multiple photons interact at the same time within the focal volume to induce a nonlinear effect. Two-photon excitation fluorescence (2PEF), predicted in 1931 by Maria Göppert-Mayer [73, 74], involves the simultaneous absorption of two infrared photons whose combined energy promotes a molecule to an excited electronic state. As two photons are required for excitation, the two-photon excited fluorescence signal intensity is proportional to the square of the excitation intensity. This nonlinear absorption occurs only at regions of high photon density, leading to molecular excitation and subsequent fluorescence only at the focal point of the objective lens [75-77]. Indeed, as the probability of two-photon absorption is extremely low, this phenomenon is only possible if the sample is excited with high power densities (MW/cm^2 to GW/cm^2). This is currently achieved using femtosecond or picosecond pulsed lasers focused down to sub-femtoliter sized volumes within the sample. As emission only occurs at the focal point, multiphoton microscopy tools do not require spatial filters and thus offer

intrinsic optical sectioning. To build 2D and 3D images, the laser focus is scanned in two or three dimensions in the sample. As the quantum mechanical selection rules for one and two-photon absorption are different, the two-photon absorption spectrum does not always mirror that of one-photon absorption. However, due to Kasha's rule, fluorescence emission occurs from the same final state, leading to largely similar emission spectra and lifetime properties.

Another major advantage of multiphoton imaging is its ability to provide increased imaging depth over single photon methods, as the infrared excitation light experiences reduced scattering and absorption in turbid tissue environments. In addition, as fluorescence excitation is confined to a sub-femtoliter portion of the object focus, the sample experiences less photobleaching as well as reduced phototoxicity.

2PEF (sometimes called TPEF) imaging has found applications in both *ex vivo* and *in vivo* human skin drug delivery studies [3, 4, 6, 7, 23, 56, 78-90], and achieves cellular-level and depth-defined visualization of exogenous fluorescent drugs. The 2PEF intensity z-profile is one of the most straightforward quantification parameters extracted from the images, and enables insight into drug delivery profiles. *In vivo* 2PEF imaging in human volunteers has limitations in terms of image acquisition speed and image field of view, but a fluorescent drug can be detected through the entire epidermis and within the uppermost 100 μm of dermis with relative ease. Using this method, Yamada *et al.* were able to directly acquire, *in vivo* on forearm skin, penetration depth data of the previously described elongated microparticles combined with tailorable nanoemulsions and arginine (see Figure 3 right). They used 6-Carboxyfluorescein (CaF) in the core droplet of tailorable nanoemulsions (TNE) in volunteers for the first time and characterized the delivery of CaF within the epidermis and uppermost dermis at 2 time-points (15 and 50 min) post application. CaF was selected as a fluorescent drug surrogate based on the similarity of size, charge and hydrophobicity characteristics to small therapeutic drugs that are classically difficult to deliver through skin. These 2PEF images support the hypothesis that EMP formulations can enhance the delivery of TNE in human skin *in vivo*. CaF 2PEF imaging was performed at an excitation wavelength of 900 nm, a wavelength at which the autofluorescence intensity of the epidermis is low (e.g. no cellular constituents are visible on the images in Figure 3 right) and 2PEF signal can mainly be attributed to exogenous drug fluorescence. When both endogenous skin constituents and exogenous fluorescent drugs have similar excitation/emission properties, fluorescence lifetime imaging can be employed provided that their fluorescence lifetime profiles are different (see section 2.4).

Furthermore, 2PEF imaging can be combined with other nonlinear imaging modalities that offer additional sources of contrast, such as second harmonic generation (SHG) and coherent Raman scattering (CRS) [91] (see Section 3.3). Demonstrations of work capitalizing on the complementary data provided by these techniques are detailed in later sections. SHG is a coherent second-order nonlinear process that, while 'Forbidden" in most compounds, can occur in special molecules and structures that exhibit what is known as non-centrosymmetry. In this type of medium, two photons can be converted into a new photon at double the original frequency, corresponding to half the original wavelength. Advantageously, both 2PEF and SHG signals can be excited using the same laser source and detected separately based on their spectral difference (red-shifted 2PEF compared to SHG). Applications of

SHG imaging in human skin drug delivery are limited to epidermis, since fibrillar collagens in the dermis generate intense SHG signals that cannot be discriminated from the SHG signals generated from exogenous compounds.

The application of SHG to drug studies was successfully demonstrated by Mohammed *et al.* using broad-spectrum sunscreen containing zinc oxide nanoparticles (ZnO NPs) [8]. This study investigated the safety and toxicity of repeated application of agglomerated ZnO NPs applied to human volunteers over 5 days by assessing the skin penetration of intact ZnO-NPs and zinc ions. Multiphoton 2PEF-FLIM of NADH and FAD was used to directly visualize viable epidermal metabolic changes and SHG imaging to assess the ZnO-NP skin penetration. Figure 4 shows representative 2PEF /SHG images of the different epidermal layers of untreated skin and skin after repeated application of vehicle, uncoated and coated ZnO-NPs. The authors found that ZnO-NPs (SHG signal in red) accumulated on the forearm skin surface and within the skin furrows but did not enter or cause cellular toxicity in the viable epidermis (no change in the NADH and FAD fluorescence lifetime parameters).

2.4. Multiphoton 2PEF-FLIM imaging

Fluorescence lifetime imaging microscopy [92] in association with 2PEF imaging brings an additional contrast mechanism for increased specificity, offering insight into the type of fluorophores contributing to the detected signal. Fluorophores with similar emission spectra can be differentiated by FLIM provided they display different fluorescence lifetimes. Fluorescence lifetime (τ) is a measure of the ensemble average time between the molecule's excitation and its return to the ground state. The fluorescence lifetime has traditionally been computed using time-domain analysis by fitting the fluorescence decay trace with multiple exponential decay functions to extract unique molecular lifetimes and their contributions. Typically, a simple molecule's fluorescence lifetime has a single exponential decay shape. Most of the exogenous fluorophores used as model drugs in skin delivery studies show this behavior, but in the human skin, the autofluorescence signal within the sub-femtoliter excitation volume comes from a variety of endogenous fluorophores and the fluorescence decay typically shows a biexponential behavior: $Photon\ count(t) = a_1 e^{-\frac{t}{\tau_1}} + a_2 e^{-\frac{t}{\tau_2}}$ where τ_1 and τ_2 are, respectively, the fast and slow lifetimes and a_1 and a_2 their amplitudes.

The skin's autofluorescence lifetime spans from hundreds of picoseconds (e.g. melanin, free NADH, bound FAD) to nanoseconds (see [93] and included references). The bi-exponential fit thus provides information on the fast and slow fluorescence lifetime and their relative amplitudes $a_1[\%] = \frac{a_1}{a_1 + a_2}$ and $a_2[\%] = \frac{a_2}{a_1 + a_2}$. One can use the images of τ_1 τ_2, a_1[%] and a_2[%] as well as combination parameters for images such as the intensity- or the amplitude-weighted averaged lifetime $\tau_{Av\ Amp} = \frac{a_1\tau_1 + a_2\tau_2}{a_1 + a_2}$ to look for differences between endogenous skin constituents and an exogenous fluorescent drug. Using this approach, Alex *et al.* recently demonstrated the feasibility of *in vivo* and *in situ* 2PEF-FLIM for the visualization of the topical drug's uptake within the human skin at daily clinical practice environment (see Figure 5) [4]. The topical drug candidate studied advantageously had a distinctly longer fluorescence lifetime than that of the surrounding skin's autofluorescence, allowing the local

distribution of the topical drug's uptake to be selectively visualized within the human skin. As 2PEF imaging is non-invasive and non-destructive, the 3D pharmacokinetics of the study drug were observed longitudinally over the course of ten days using this FLIM approach.

Although the fluorescence lifetime is independent of the fluorophore concentration, it depends on the local microenvironment of the molecule. These variables include pH, binding status, and molecular conformational changes. Furthermore, the human skin's autofluorescence is highly heterogeneous, both spatially within individuals and between individuals [94]. Such variables can alter a molecule's fluorescence lifetime, making it difficult to determine the exponential decay functions needed to accurately extract fluorescence lifetime information. In this case, the phasor approach to FLIM is highly advantageous as it does not require *a priori* knowledge of the sample for data analysis [95].

In phasor analysis, the fluorescence decay trace in each pixel is mathematically transformed into a pair of phasor coordinates, G and S that represents the cosine and sine components of a Fourier transform. All possible phasor coordinates of a single exponential decay in the phasor plot lie on the so-called universal semicircle going from point (1,0) to point (0,0), corresponding respectively to $\tau = 0$ and $\tau = \infty$ (see Figure 6). For a mixture of two distinct single lifetime components in an image pixel, the phasor coordinates lie inside the universal semicircle, rather than on its boundary, and reside along a line connecting two distinct lifetime points. In the case of multiple fluorescent components colocalized within the same pixel, the phasor coordinate is the sum of the independent phasor coordinates of each fluorescence component. The relative contributions for each pixel can be calculated by computing the relative distance from the pixel's phasor to the phasor clusters of the individual known fluorescent species. This feature is highly beneficial when visualizing and quantifying multiple fluorescent topical drugs co-delivered into the skin.

This approach was recently used by Osseiran *et al.* to study fluorescent chemical sunfilters that were found to penetrate within the *stratum corneum* on *ex vivo* human skin and cause measurable redox shifts [20]. These tools were also used to visualize the delivery of topically applied minocycline within *ex vivo* human facial skin [23]. In this study, minocycline advantageously had a shorter lifetime (400-500 ps) than that of skin's autofluorescence (1.5 ns). However, extraction of the minocycline signal from autofluorescence was complicated by the large heterogenous spread in both contributions. As shown in Figure 7, the phasor cluster of minocycline is located within the universal semicircle instead of its boundary, indicating minocycline sample itself contains multiple fluorescence lifetime contributions. Experiments revealed that these contributions arose from a number of factors, including tissue water content, the degree of magnesium ion chelation, and pH. However, by obtaining the phasor cluster references of the topical drug and skin autofluorescence, phasor analysis enabled extraction of the local minocycline contribution.

3. Vibrational spectroscopic imaging methods

Vibrational spectroscopic imaging techniques are unique in their ability to visualize and quantify molecular species by their intrinsic molecular structures. Molecular structures give rise to unique molecular vibrations; as molecules are a sum of individual structures, every

molecule can be associated with a collection or “fingerprint” of associated vibrational frequencies that together comprise a spectrum. Vibrational spectroscopy and, by extension, vibrational spectroscopic imaging uses these unique vibrational spectra to identify, locate, and quantify specific chemical species within samples. Importantly, these vibrational frequencies are intrinsic to each molecular structure, allowing for detection and imaging of molecules without the need for exogenous labeling. When paired with microscopy tools, vibrational spectroscopic methods can provide non-invasive, sub-cellular resolution imaging deep within tissue *in vivo* lor pharmacokinetic (PK) measurements.

There are two major classes of vibrational spectroscopic imaging: techniques based on light absorption and techniques based on light scattering. Light absorption approaches make use of near-infrared and infrared (IR) light to directly excite molecules to higher vibrational modes. Infrared spectroscopy and spectroscopic imaging pass a range of infrared wavelengths through a sample and determine the absorption spectrum at individual locations. The absorption spectra can then be used to map out molecular species. Infrared spectroscopy and imaging can be carried out in reflection or transmission modes and can suffer from water absorption, such that they are often used on thinly sliced or sectioned tissues.

Light scattering methods take advantage of the Raman effect, discovered in 1928 by the Nobel-prize winning scientist C.V. Raman. In Raman scattering, photons interact with a molecule’s vibration scatter with unique quanta of vibrational energy. A wide range of spectroscopic and microscopic techniques, such as spontaneous Raman spectroscopy, coherent anti-Stokes Raman scattering (CARS) microscopy and stimulated Raman scattering (SRS) microscopy, have been developed and used for a broad range of biological and biomedical applications [96-98]. As Raman-based methods make use of scattered light, they can be used in epi-collection configurations compatible with *in vivo* imaging. Moreover, since the Raman effect involves gain, loss, or interactions with quanta of vibrational energy, Raman spectroscopy and imaging methods can be carried out using UV, visible, and near-infrared light, allowing for resonance-enhanced Raman as well as Raman approaches to image deep within tissue.

3.1. Infrared Spectroscopy and Microspectroscopy

The existence of light beyond the red wavelengths of the visible spectrum was first discovered in the 19th century by Friedrich Wilhelm Herschel [99]. Using diffracted sunlight and removing the visible wavelengths, he was able to induce heating with this newly discovered infrared light and hypothesized a common origin for both visible light and heat radiation. During these experiments he also studied the transmission of infrared light through different materials, but it was not until the mid-20th century, with innovative electronics that enabled the use of automated spectrometers, that infrared adsorption was studied in more detail [100, 101]. Since its development, IR spectroscopy has become a widely used analytical tool to assess chemical compounds for industrial purposes and later applied to the pharmaceutical and food industries [102]. Building upon developments in other fields, IR techniques have been implemented to analyze cells and tissues [103] and for medical diagnosis and screening purposes for applications ranging from diabetes to cancer

research [104, 105]. For cancer research, vibrational spectroscopy has been demonstrated for the analysis and mapping single cells and tissues [106, 107]. Recent studies have explored the use of IR tools for the detection of glucose concentration *in vivo* [108]. While IR wavelengths are prone to substantial absorption by water, IR spectroscopy can still be applied superficially *in vivo* as a non-invasive tool to study the structure and composition of human skin and its barrier function.

In vibrational spectroscopy, the most commonly used unit is the wavenumber, with units of reciprocal centimeter (cm^{-1}), which is proportional to light frequency and therefore energy. Infrared photons in near, mid and far-IR wavelengths whose energies match that of vibrational level transitions are absorbed when passing through a sample. Infrared spectra display this loss of photons to the sample in an infrared absorption spectrum. Quantum mechanical selection rules favor the absorption of single vibrational quanta of energy, such that infrared absorption spectra are dominated by single infrared absorption. While quantum mechanically 'forbidden", overtone vibrational transitions can occur, where a molecule absorbs two or more quanta at once. However, these absorption events are far less common, but they can be measured and have optical effects in tissue such as the second- and third-overtone vibrations that limit the penetration of near-infrared light at certain wavelengths in tissue.

IR spectroscopy can be used for characterization of endogenous biological molecules such as water, proteins, nucleic acids, lipids and carbohydrates [109], as well as detection of structural changes which occur in diseased states. Clinical biomarkers have been investigated primarily in the mid-IR absorbance range to study genomics [109] and proteomics [110]. The far-IR (also known as thermal IR) also offers non-contact evaluation of dermatological complications such as burn wound depths [111]. An example of the information available via IR spectroscopy is shown in Figure 8 (B & C) from a histological section of skin (A) (adapted from [112]).

The protein-related amide I and amide II bands at 1650 and 1550 cm^{-1} are clearly visible, as well as the lipid-related bands at 1735, 2850 and 2920 cm^{-1}. The signals below 1500 cm^{-1} arise due to asymmetric and symmetric CH_3 bending vibrations from peptides and proteins (1457 and 1400 cm^{-1}), the asymmetric and symmetric stretching of ionized PO^{2-} (1240 and 1075 cm^{-1}) related to DNA and RNA molecules, and the vibrational modes of CH_2OH groups and C–O stretching along with C–O bending of the C–OH groups in carbohydrates (1025 and 1045 cm^{-1}) [105].

IR microscopy, or IR microspectroscopy, is a specific version of light microscopy where the light source transmits IR wavelengths of light. Seminal work by Potts, Francoeur, and colleagues at UCSF established many of the application of IR microscopy to skin imaging, including studies focused on lipid composition [113, 114] and the transport of molecules through the skin [115, 116]. These and other investigation of conditions associated with compromised skin structure have been well suited to IR microscopy [117]. While upper layers like the *stratum corneum* of the skin are easier to visualize with infrared methods, interrogating deeper layers is optically challenging due to photon scattering and absorption, resulting in poor light throughput [118]. Tissue assessment using IR absorption can provide

information regarding the depth of the intact tissue [119], however, IR imaging does lack 3D sectioning capabilities. To overcome this need, modalities like Fourier transform infrared (FT-IR) spectroscopy and attenuated total reflection-Fourier transform infrared (ATR-FTIR) spectroscopy have been implemented to offer depth profiling [120].

ATR-FTIR can also integrate other spectroscopy and microscopy techniques like Raman spectroscopy [121], atomic force microscopy (AFM) [122, 123] and scattering scanning near field microscopy (s-SNOM) [124]. For example, an ATR-FTIR and Raman spectroscopy approach was recently used by Balazs *et al.* where they combined the delivery of a lyotropic liquid crystal genistein-based formulation (LLC-GEN) with electroporation (EP) . They used ATR-FTIR and Raman spectroscopy to examine the synergistic effect of EP on hairless mouse skin *ex vivo* and *in vivo*. These studies demonstrated that the LLC-GEN formulation was an effective transdermal drug transporter and the combination of this nanocarrier system with EP enhanced the delivery and effectiveness of the drug [125]. Moreover, ATR-FTIR, when combined with AFM, offers nanoscale imaging below the diffraction limit. Here, the nanoscale spatial resolution of the AFM tip response is tied with the infrared light interaction: the signal collection is dependent on thermal expansion and relaxation of material after light absorption [120]. In another study of chemical penetration enhancers by Zhang *et al.*, an ATR-FTIR and AFM combination system was used to demonstrate the significant skin permeation promotion profiles of imidazolium ionic liquids [122]. Furthermore, while infrared imaging is used frequently *ex vivo* to look at lateral diffusion of chemical formulas such as acyl chain perdeuterated oleic acid (OA-d) [126], experiments can be readily accompanied by *in vivo* evaluation. One such example are studies of cyanophenol [127], hydroxypropyl-β-cyclodextrin-grafted polyethyleneimine (HP-β-CD–PEI) with vitamin B12 as a model drug [128], and the model drug flufenamic acid with deuterated liposomal drug delivery system [129]. Excellent reviews detailing developments in IR imaging frameworks [120], fundamental technologies [130] and applications [121] are available.

One benefit of the specificity of vibrational microscopy techniques such as those based on IR is that the different vibrational signals originating from distinct molecules can be used to extract quantitative molecular concentration information in the context of tissue structures [112]. For example, the water content in skin *in vivo* can be estimated using ATR-FTIR spectroscopy, by analyzing absorption at 1640 cm^{-1} and between 3225 cm^{-1} and 3615 cm_{-1} [131]. Lipid vibrational signals can be used to gain information regarding the lipid content and organization within the *stratum corneum*. In this skin layer, lipids can be in orthorhombic or hexagonal ordered phases, as well as in a liquid-crystalline, disordered phase. These two phases have unique vibrational signatures that can be studied using IR spectroscopy [132]. Using the splitting of the CH_2 rocking vibrations (720 and 729 cm^{-1}) which is characteristic for orthorhombic phases, it was shown that phase transitions can be induced in isolated *stratum corneum* using heat [133]. A complementary approach based on the analysis of the width of the second-derivative of spectra in the region between 1475–1460 cm^{-1} was developed for *in vivo* application with ATR-FTIR spectroscopy [134]. The packing of lipids and their concentration can be related to changes in the skin barrier function [135] making IR a potent method to follow structural changes after application of permeation enhancers. In a screening study, different penetration enhancers and their effect

on skin penetration were correlated with the CH_2 symmetric stretching mode at 2850 cm^{-1}, which enabled the design of new penetration enhancers expected to reduced irritation response [136].

If a topically applied molecule has a specific vibrational band that does not coincide with one of the bands observed in skin, IR spectroscopy can be used to follow drug delivery. An exemplary experiment is shown in Figure 8 [137], where the authors followed the penetration of the deuterated moleculel-palmitoyl-d_{31}, 2-oleoylphosphatidylcholine (P-d_{31}OPC) along a histological cut of pig skin. The CD_2 stretching modes from DPPC observed at approx. 2090 and 2190 cm^{-1} lies within the "silent" spectral region and can therefore be used as a fingerprint for the molecule. IR microscopy was also used to follow the penetration of deuterated propylene glycol and deuterated dimethyl sulfoxide (DMSO) on histological cuts [138], and a similar approach used to follow the uptake of chitosan [139].

Despite the demonstrated sensitivity of IR techniques to specific constituents both within native skin tissues and exogenous chemicals, fundamental limitations hinder some biomedical applications of this spectroscopic analysis. Water adsorption remains a significant challenge, limiting *in vivo* applications. As IR absorption is non-negligible in tissues, signal attenuation can reduce efficient collection and invalidate Beer-Lambert law assumptions [129]. Furthermore, the appreciable IR absorption typically limits IR backscattering to only the upper layers of the *stratum corneum* with sufficient intensity for imaging [140]. Combinations of techniques, such as nanoscale IR imaging based on AFM may one day have value beyond mapping composition and structure of lipids within the *stratum corneum* at high resolution. [123]

3.2. Confocal Raman spectroscopy

When a molecule scatters light, most of the photons are scattered elastically, in a process known as Rayleigh scattering. During this process, the energy of the scattered photons is the same as the incident photons. However, a small fraction of light ($1/10^7$) can be inelastically scattered at unique, different frequencies through interactions with vibrational modes of the molecules. The scattered photons can leave with gains or losses in energy equal to vibrational quanta of energy, and therefore carry information regarding molecular structure. This inelastic scattering mechanism is known as spontaneous Raman scattering, where the dependence of the signal is given by [141] $I_{Raman} \propto Im[\chi_R^{(3)}]$.

The Raman scattering intensity I_{Raman} has a linear relation with the imaginary part of $\chi_R^{(3)}$, and it is only sensitive to the resonant part of the material response. Those properties result in a theoretically high signal-to-noise ratio in Raman spectroscopy and a linear relation with molecular concentration. In practice, Raman effect can be rather weak due to the small fraction of light that is Raman scattered, resulting in the need for long acquisition periods [142]. Measuring a spectrum at a single point in a sample can require seconds, while acquiring a Raman spectral image can take hours [142]. Depending on the wavelength of light used and the tissue interrogated, Raman scattering is often accompanied by tissue autofluorescence that can be many times greater than the Raman signal itself. Special data

analysis methods are typically employed to remove unwanted spectral contributions and interpret the complex spectral information [143].

For applications in drug delivery, spontaneous Raman spectroscopy is often integrated with a confocal optical path to obtain spatially-resolved information. As such, the spatial resolution of confocal Raman scattering systems can range from hundreds of nanometers (for UV and visible excitation light with high NA objectives) to micrometers (near-infrared and low NA lenses) [142]. In combination with infrared laser excitation, confocal Raman allows spectral acquisitions at depths of tens of micrometers [144]. Deeper tissue imaging can be possible if the confocal pinhole is enlarged: by compromising depth resolution to 10-20 μm, Bonnist *et al.* reported a direct confocal Raman measurement up to 300 μm deep using a long working distance objective [145]. This ability to detect materials by their vibrational spectral signature deep within skin has made confocal Raman of special interest in drug delivery research as it enables non-invasive evaluation of compound penetration behaviors [146].

Confocal Raman spectroscopy can be adapted for application using classical Franz diffusion cells by making use of skin explants. This approach can be used to glean pharmacokinetic data alongside traditional Franz cell measurements. Forster *et al.* used this method for tracking cosmetic ingredient penetration in excised skin after 24 hours' treatment [147]. To overcome the limitation of depth, freeze-dry excised skin samples can be further prepared after the treatment on a Franz diffusion cell. For example, this method has been used for detecting the penetration of Metronidazole [148] and hyaluronic acid of different molecular weights (see Figure 9) [149] up to several millimeters depth. By freeze-drying skin samples at defined time points, molecular penetration can be observed kinetically at a quantitative level [150].

As Raman spectral measurements require relatively long integration times, *in vivo* measurements can be complicated due to natural body motions, such as breathing and heartbeats. *In vivo* Raman imaging thus requires careful stabilization of the subject or specific body region being interrogated. One commonly used system is an inverted microscope, such as reported by Caspers *et al.* [144, 151, 152], which has been commercialized for skin research [153, 154]. For example, it has been used to observe the delivery of retinol [155, 156], carotenoids [157], various oils [158, 159] and vitamin derivatives [160] in human skin *in vivo*. Furthermore, dynamic observation of molecular penetration can be also performed *in vivo*. Pot *et al.* reported real-time monitoring of p-phenylenediamine penetration [161]. Santos *et al.* introduced dynamic analysis of retinyl acetate delivery into *stratum corneum* [162]. The design of this commercial system is unfortunately limited to assessing the skin of limbs placed over the objective lens, meaning that most of the studies above were performed on human forearms. To overcome this limitation, other *in vivo* systems were built to make use of a flexible probe connected via optical fibers [163]. While this design is in principle more adaptable to assess a variety of body zones, the stability of the system can be challenging. To stabilize the contact between objective and skin surface, a cover glass is often placed on the surface of the skin. For added depth resolution, oil immersion objectives can be employed. It should be noted, however, that an occlusive effect can be caused by the contact measurement, as Raman measurements

with this system can take a minute or longer. To avoid occlusion, air objectives can be used to eliminate contact, with the associated loss of acquisition stability.

As we have already mentioned, theoretically spontaneous Raman response has linear relation with molecular concentration. However, in a scattering medium such as skin, the light attenuation in depth has a strong effect on both incident light and collected signal. To well estimate this energy loss in depth profiling, an endogenous reference is commonly used. Based on the assumption that the reference component, such as protein (C-H bend or CH3 stretching) [148, 151, 152], is homogeneously presented in skin, the relative intensity of a drug to the reference component intensity can be used for signal attenuation correction. However, we have to keep in mind that this assumption is not totally correct due to the complex skin structure. Besides, Franzen *et al.* has established a mathematical algorithm to correct Raman signal attenuation in human skin [164]. They have developed a skin surrogate to simulate the optical properties of human skin, for investigation of Raman signal attenuation. Although they have included most of human *stratum corneum* compositions in this model, the variation between skin types *in vivo* and the presence of melanin in depth are not considered. For precise quantitative analysis of drug uptake in skin, data analysis method is still a challenging topic due to the complexity of skin structure and compositions, as well as, the huge variation of individuals caused by origins and life styles.

It is worth noting that there are many efforts seeking to improve the data acquisition rate for spontaneous Raman tools such as confocal Raman. A major innovation is the application of compressive Raman spectroscopy technology [165-167]. Unlike conventional methods, where a complete vibrational Raman spectrum per spatial pixel is acquired, compressive Raman technology applies a known ‘mask’ of only interesting frequency regions when taking a hyperspectral image. This encodes only useful information in the measurement. Soldevila *et al.* recently used a compressive spectrometer in combination with computational technique, to reduce the effective acquisition time to 0.4 ms/pixel for lipid-protein imaging of tissue [168]. It is anticipated that this approach can be readily applied to drug imaging and pharmacokinetic studies.

3.3. Coherent Raman scattering microscopies: CARS and SRS

Coherent Raman scattering methods offer significantly greater signal and speed over traditional spontaneous Raman methods, allowing for vibrational imaging of pharmacokinetics and pharmacodynamics *in vivo* up to video-rate speeds. These advantages come with the trade-off of added complexity: coherent Raman processes are stimulated and therefore require two laser light fields, called “pump” and “Stokes”. In order to “tune” into a molecular vibration of interest, the difference frequency between these two laser colors must be adjusted to match a molecular vibration or set of molecular vibrations. In coherent Raman imaging, the frequency difference between the lasers creates a coherent, stimulated condition that gives rise to signals that are orders of magnitude greater than the conventional spontaneous Raman. By using a pair of lasers to specifically tune into the molecular vibrations that arise from specific chemical structures, CRS allows for the biochemically sensitive and non-destructive detection of native molecular species *in vivo* at video-rate speeds [169].

There are two main coherent Raman imaging methods currently in use for the visualization of drugs and tissues: CARS and SRS. These complementary processes occur simultaneously within the sample and can be measured via different detection schemes. In CARS, the presence of a molecular vibration gives rise to a photon at the anti-Stokes frequency [170]. In SRS, a modulation transfer scheme is used to detect the transfer of energy from the Stokes beam to the pump beam that occurs in the presence of a resonant vibrational mode. SRS is advantageous in chemical imaging over CARS, as the CARS signal is mixed with and contaminated by a non-resonant contribution [170-172]. CARS can still be extremely useful in tissue imaging, in particular, in revealing tissue structure.

Coherent Raman imaging is most typically carried out using picosecond pulses [170], whose bandwidths match the linewidth of typical Raman vibrational modes [173]. In this narrowband configuration, the frequency difference between the laser must be adjusted sequentially to tune into each molecular vibration. While this approach has traditionally been slow, new advances in fiber laser technology now allow for rapid tuning within microseconds [174], enabling multiband coherent Raman imaging at high speeds with high spectral selectivity.

Broadband light sources can indeed be used for coherent Raman imaging. Broadband methods can be used to collect entire hyperspectral images, similar to what is done in spontaneous Raman imaging, where each pixel contains an entire spectrum [175]. These approaches are data-rich, but slower than single-band imaging, sometimes requiring minutes per image. In 2012, Ozeki *et al.* [176] and Zhang *et al.* [177] developed hyperspectral SRS imaging techniques that use both a picosecond and a femtosecond laser together, achieving high spectral resolution over a narrow wavelength range of ~220 cm^{-1} in the high wavenumber region. Figueroa *et al.* reported a hyperspectral SRS instrument based on parabolic fiber amplification, which provided more than 600 cm^{-1} spectral coverage and ~10 cm^{-1} spectral resolution [178]. It is worth noting that coherent Raman imaging and spontaneous Raman spectroscopy can be carried out on the same optical instrument for high speed imaging and pinpoint Raman spectral acquisition. [179-181].

Femtosecond systems can be made compatible for narrowband-like imaging through a method known as temporal focusing [182], where the pump and Stokes beams are sent through dispersive media to impart a linear chirp. This chirp can be set such that the two pulses have the same rate change in frequency over time, creating a condition where the two pulses have a constant frequency difference throughout the pulse width. This temporal focusing approach can be advantageous for tuning, as small changes in the temporal delay between the pulses act to change the effective frequency difference, enabling near-narrowband spectral resolution and simple, but limited, tuning range. Recent work by the Cheng group has worked to transform this method into a high-speed hyperspectral imaging tool, where coherent Raman hyperspectral stakes can be acquired over 100-200 wavenumbers of spectral bandwidth [183].

As CRS is a microscopic imaging technique, it can be used to follow spatiotemporal changes within tissue at subcellular scales to reveal underlying chemical dynamics [184]. Prior research has demonstrated that CRS can quantitatively track unlabeled drugs via their unique

chemical structures in real time for both *in vivo* drug and formulation testing [185]. The most common means of visualizing specific drugs or actives within skin has been to tune into unique molecular vibrations that arise from chemical structures not found *in vivo*. This is of great importance, as the contrast in coherent Raman imaging arises from molecular vibrations in a sample; it is difficult to visualize and quantify a molecule of interest if it shares all its vibrational modes with tissue. Examples of unique, or bio-orthogonal, molecular structures include alkyne groups, nitriles, conjugated structures such as chains of vinyl groups, and ring structures containing heteroatoms such as like piperazines. Many of these vibrational modes fall within the so-called “silent region” of the vibrational spectrum, a span from 2000 wavenumbers to 2700 wavenumbers where there are essentially no Raman active modes arising from biological samples. Coherent Raman imaging experiments that target silent-region vibrational models, such as alkynes, benefit as there are no background contributions from the tissue itself [170-172].

For molecules that do not have unique vibrational modes, isotope labelling can be employed to add specific Raman contrast The most common isotope labelling approach is to swap carbon-hydrogen bonds for carbon-deuterium bonds; this results in a massive vibrational band energy shift. While aliphatic and aromatic C-H stretching vibrations lie in the 2800-3200 cm^{-1} range, the heavier C-D counterpart is shifted to within the silent region between approximately 2100 and 2250 wavenumbers [186]. This can be highly advantageous, as it enables the direct observation of otherwise undetectable molecules and can be extended to a range of therapeutics including antibodies and peptides. Other labels have been recently developed, including the so-called “carbow” range of Raman labels that make use of modified alkyne tags. This approach can enable multiplexed imaging of numerous labelled molecules [187].

In a review article published in 2016, Tipping *et al.* surveyed many of the advancements in the use of SRS in the general field of drug discovery [188]. While the imaging of drugs in cell culture systems had previously been carried out with CARS [189], the non-resonant background contribution in the CARS signal and the CARS quadratic signal dependence on chemical concentration made PK imaging challenging. The non-resonant contribution leads to substantial challenges in interpreting and quantifying CARS signal for anything other than well-isolated vibrational bands. The quadratic signal dependence can be compensated for in certain experimental conditions, but this requires the additional complexity of a third ultrafast, synchronized laser in the imaging setup, and the spectral interpretation challenges remain [172, 190, 191]. Quantitative analysis is difficult to achieve with CARS given these challenges, though the non-resonant background can potentially be used as a reference for compensating for depth-dependent changes in signal intensity. Using this approach, CARS microscopy was used to image the penetration of high concentrations of deuterated glycerin in skin *ex vivo* and *in vivo* [190, 191].

SRS, in contrast, is not contaminated by a background signal, has signal that is linear with molecular concentration, and has spectra nearly identical to that of spontaneous Raman. This makes SRS a potentially ideal approach for quantifying the uptake of drugs in skin. All-in-one SRS light sources can be purchased commercially, allowing for turnkey operation by biologists. One of the first pioneering applications of coherent Raman imaging in PK was

carried out by Freudiger *et al.*, who showed that SRS could be used to image drug delivery into skin [192]. They demonstrated the three-dimensional visualization of retinoic acid, dissolved in the carrier DMSO, into mouse. Saar *et al.* explored the use of SRS to visualize the simultaneous penetration of the drug ketoprofen in a deuterated carrier into skin over time (Figure 10) [193]. In this work, ketoprofen was specifically imaged via the stretching vibration of its benzophenone structure, while the propylene glycol carrier was deuterium-labeled to facilitate imaging via C-D stretching vibrations. Work by Belsey *et al.* showed the use of CARS, SRS, and 2PEF in the visualization and depth profiling of ibuprofen, a propylene glycol-d8 solvent, and fluorescein-labelled microparticles in normal and ablated porcine skin over a few hours, observing simultaneously both drug deposition and crystallization of the drug within the skin [91]. A recent study by Wei *et al.* imaged the antifungal drug terbinafine via its alkyne group in the skin of mouse ears [194], visualizing a high correlation of this lipophilic drug with lipid distribution in the tissue

Despite the successful applications of CRS, quantitative computational analysis of PK within the skin has remained a challenging due to the heterogeneous behavior of drugs within the tissue's complex structure. Recently, Feizpour *el al.* developed a method that leveraged CRS for investigating topical anti-inflammatory drug PK in mouse skin [195]. This method performed multi-depth, time-resolved imaging using SRS microscopy and included a quantitative image analysis approach that made use of Convolutional Neural Networks (CNNs) to identify structures, cells and cell types in skin. Figure 11 shows the use of SRS for imaging 4 various compartments at different depths (up to 100 μm) in mouse skin. A U-Net [196] was used for the segmentation of lipid-rich from water-rich areas of the images and the extraction of relative drug uptake at *stratum corneum* when the drug is dissolved in two different vehicles.

While coherent Raman imaging does enable chemically-specific, direct imaging of pharmacokinetics, it does suffer from a few drawbacks that makes its application as a universal drug-imaging tool challenging. CARS and SRS work well for concentrations of molecules that are relatively high, with both methods having lower-concentration limits in the 100 micromolar range for routine imaging experiments of silent-region vibrational bands. The situation can become worse when attempting to image molecules whose modes are within the fingerprint or high-wavenumber regions of the Raman spectrum: here tissue signal contributions can overwhelm the molecular signal of interest. There have been numerous efforts to overcome these issues, and many researchers in this space are investigating new means to boost imaging and detection sensitivity [192, 197, 198]. At the moment, however, these sensitivity limits constrain the application of coherent Raman methods from finding utility in PK studies, in particular those that would seek to follow tissue drug uptake of systemic drugs.

An additional challenge exists to extend coherent Raman imaging as a general-purpose tool for all possible drugs. The discussion above largely focused on drugs that either have unique vibrational modes or have been isotope labelled. The majority of drugs do not have unique modes, and isotope labelling, while acceptable in many pre-clinical studies, can be challenging, expensive, and inappropriate for many clinical studies. One potential route towards building a more general-purpose CRI PK imaging tool would be gather

hyperspectral data. However, as mentioned earlier, most coherent Raman spectroscopy methods are either too slow or are limited in tuning range. There are several efforts to overcome this limitation, with many researchers pushing the state of the art in hyperspectral coherent Raman imaging. Particularly promising for this purpose is a new generation of fiber lasers that can be rapidly tuned to visualize numerous bands throughout the Raman spectrum to enable visualization of a far greater number of drug species in tissue [174].

4. Methods comparison

Understanding the spatial and temporal distributions of pharmaceutical and cosmetic compounds within the skin has become increasingly important during product development. In this regard, the FDA supports the development and the evaluation of imaging technologies for bioequivalence studies of topical products. All these methods can help in characterizing the uptake of specific drugs within human skin and even follow a drug's penetration and residency within human skin. The imaging methods described above make use of light to interrogate skin, many of which can be configured for non-invasive imaging. These approaches are also advantageously non-destructive, enabling their use repeatedly to follow changes in drug and chemical uptake over time in the same tissue sample, specimen, or individual. As such, many of the optical tools discussed can be used *in vitro*, *ex vivo* and *in vivo* with the ability to be directly applied to subjects and patients in the clinic for real-time pharmacokinetic and pharmacodynamic studies.

Table 1 summarizes the performance of each method in skin drug delivery studies according to their spatial resolution, sensitivity, specificity and the extracted semi- or quantitative information. All these imaging technologies are already maturely commercialized. Moreover, some of them such as multiphoton 2PEF/FLIM/SHG imaging are available as medical devices approved for their use on human skin *in vivo* and CRS imaging devices that can be used for human studies are also coming on the market.

Each of these approaches have their own strengths and weaknesses. 2PEF, along with FLIM and second harmonic generation microscopies, are non-invasive methods that can be readily applied to human skin drug delivery studies. The skin distribution profile of cosmetic and pharmaceutic ingredients with natural fluorescence or non-linear optical properties can be assessed using these methods in 2D or 3D, on cultured cells, in *ex vivo* tissues, and *in vivo* in human skin [26, 199-205]. By incorporating exogenous fluorophores as model drugs, these technologies have also found applications in the development of transdermal drug delivery systems. Fluorescence approaches can be highly sensitive to lower, nano- and pico-molar quantities chromophores, but require that the compound or drug of interest be fluorescent or have special non-linear properties. Fluorescence methods also must contend with the strong native autofluorescence of skin. While technologies such as FLIM can be used to separate out some fluorophores from this background, the ultimate sensitivity of a fluorescence imaging experiment can be severely limited by the autofluorescence emission of skin itself. It should be noted that FLIM imaging of endogenous fluorophores can be used to extract information on the cellular metabolic activity. Thus, one can non-invasively and simultaneously assess the drug's penetration and its effects on the skin cellular metabolic activity and, in the case of drug delivery systems, their safety of use [20].

Multiphoton fluorescence methods, by using infrared light, can achieve deeper tissue penetration than that of single-photon fluorescence excitation configurations such as confocal, but the maximum skin imaging depth of fluorescence is measured in hundreds of micrometers. For strong fluorophores, video-rate and higher imaging speeds are possible, enabling rapid pharmacokinetic imaging in living tissue.

It is important to note that fluorescence methods are largely semi-quantitative, providing measurement of the local emission contributions of images, as the local tissue environment (e.g. pH, water content, etc.) can modulate fluorescence emission properties. The drug's signal must first be separated from the skin signal, either spectrally or based on the fluorescence lifetime. 3D automatic segmentation of epidermal and dermal compartments from 2PEF/SHG skin images [37], can be used to determine uptake, as well as melanin, elastin, fibrillar collagen content, and the location of the dermal-epidermal junction (DEJ) [25, 40, 63]. This type of information enables semi-quantitative measures of drug uptake within unique skin compartments across different skin types and different individuals.

Infrared and confocal Raman approaches advantageously can be used to visualize essentially any potential drug or compound, as they collect complete molecular vibrational spectra Infrared imaging is largely limited to *ex vivo* samples and the skin surface due to water absorption of the infrared light. The use of infrared light also acts to reduce the spatial resolution of infrared microspectroscopy to micrometer scales. Confocal Raman, which is routinely performed in animals and humans, can be used to acquire spectra down to approximately one to two hundred micrometers deep in skin. This single-point, spectral acquisition approach can be rapid for time-resolved measurements, however, the weakness of the spontaneous Raman effect means that acquiring Raman images can take hours to days. This makes confocal Raman imaging ideal for either *ex vivo* sample imaging or for acquiring point-location spectra *in vivo*. The sensitivity of both infrared and confocal Raman is set by the spectral contrast of the molecule of interest versus the contribution from the skin tissue itself.

Rounding out the list of tools is coherent Raman imaging, which makes use of vibrational spectral information in a multiphoton-like configuration. This gives it the advantage of video-rate or higher temporal resolution and subcellular resolution at depths hundreds of micrometers deep within tissue. Current coherent Raman methods are restricted to targeting unique or bio-orthogonal vibrational bands, though the fast-evolving nature of the coherent Raman research community will likely improve on this limitation in the years to come. CARS microscopy has reduced sensitivity compared to SRS microscopy due to the presence of a non-resonant background contribution inherent to the CARS process. The signal in CARS also scales with the square of the concentration of a given molecular specie. These considerations make SRS the clear optimal choice for imaging drug or compound uptake within tissues such as skin. The sensitivity of SRS is restricted to the upper 100's of micromolar to millimolar regime for unique and bio-orthogonal vibrational bands, depending on the molecule of interest. Like spontaneous Raman tools, the in-practice sensitivity results from a balance between the signal contributions from the molecule versus that of the background skin tissue.

An important consideration to weigh when choosing a modality for analysis balances the cost and complexity of the tools used to obtain the relevant data. These considerations vary greatly across the imaging modalities discussed, from commercial systems to complicated research-grade technologies. Conventional and confocal fluorescence microscopes require little expertise to operate, with many commercial systems available from a range of vendors including Biotek, Leica, Nikon, Olympus, Zeiss. Multiphoton fluorescence and FLIM systems typically require more expertise and system interaction. While a few systems are marketed as turn-key, most are based on more conventional confocal laser scanning microscope systems with integrated ultrafast laser sources and additional detector channels. Aligning and coupling a laser source into an available microscope beam path is typically the primary source of complexity associated with data collection for these modalities, along with identifying correct imaging parameters for lifetime acquisitions. The ultrafast tunable lasers used for imaging are provided by a few companies including Coherent and Spectra-Physics at costs similar to or exceeding that of the microscope itself.

Vibrational imaging similarly spans a wide spectrum of both cost and complexity. Infrared microscope systems are commercially available from suppliers such as Agilent, Bruker, PerkinElmer, and ThermoFisher. These compact, benchtop instruments are turnkey with fully integrated components. Similarly, spontaneous Raman microspectroscpy systems are commercially available fully packaged with excitation lasers, microscope control, and detectors from several vendors (*ca.* Bruker, Horiba, Renishaw, and WiTec). These systems are similarly costly due to the needed stable laser sources and low noise detectors integrated to collect the weak Raman scattering signals. Similar to multiphoton fluorescence systems, coherent Raman imaging systems are high cost and high complexity instruments. While there are a few commercial systems on the market, most systems are research grade. Jenlab manufactures a 2PEF/SHG/FLIM imaging system for *in vivo* human skin studies that additionally offers CARS, but not SRS, functionality. The primary cost again originates from the need for a single dual-output, or two single-output ultrafast lasers, at least one of which should be tunable. These lasers can similarly be integrated into confocal laser scanning microscopes to utilize existing system features for image acquisition.

While these cost and complexity considerations cover the implementation and operation of the imaging systems, further thought must be paid to the analysis and interpretation of this equipment, especially for research grade, spectroscopic systems that are capable of rapidly producing large quantities of data within a single imaging session. Advanced analysis software suites vary widely by application and are beyond the scope of this review. However, once imaging parameters and analysis procedures for an application have been identified, these techniques can be easily and directly applied to a wide variety of new samples for investigation.

5. Discussion

In Part I and Part II of this review, we introduced methods and toolkits for detecting, imaging, and quantifying the uptake of drugs and compounds in the skin. These approaches include those that require specific labelling of a given compound (e.g. autoradiography) and those that are meant to work with native, unmodified species (e.g. MALDI mass

spectrometry, Raman). The toolkits can be applied to biopsy specimens (e.g. SIMS) and in living subjects (e.g. Raman, multiphoton 2PEF/FLIM/SHG and coherent Raman). Some approaches offer subcellular resolution (e.g. SIMS and fluorescence), while others are more optimized for cellular-sized features (e.g. MALDI, infrared). This wide range of toolkits and capabilities present array of choices that can make selecting the right method challenging.

Figure 12 presents a decision tree aimed at guiding experiments towards the most optimal imaging method. Molecular species that are fluorescent are typically the readily imaged *ex vivo* to *in vivo*, though it is noted that these approaches are semi-quantitative and may not have great enough specificity due to interference from other, potentially endogenous, fluorophores. Molecules with non-linear optical properties such as the second harmonic generation can provide increased specificity and no interference from the endogenous fluorescent skin constituents, but SHG imaging applications will be limited to epidermis layer, since fibrillar collagens in the dermis generate intense SHG signals that cannot be discriminated from the ones of exogenous molecules. If a molecule of interest has a vibrational signature, either a spectral fingerprint or a unique vibrational mode, vibrational imaging tools can be employed for quantitative imaging in skin. If temporal resolution is critical for a given experiment, coherent Raman offers real-time imaging speeds, with confocal Raman and infrared imaging requiring many minutes to hours to collect vibrational imaging data. If fluorescence, SHG and vibrational approaches are either not possible, or do not have the sensitivity required, mass spectral techniques are the best next approach, offering two different spatial resolution capabilities. Finally, if the molecule of interest is not amenable to mass spectrometry or if higher sensitivity is required, autoradiographic labelling is performed.

It should be noted that this decision tree is for the simplest experimental case of investigating a single drug or compound of interest. Many more considerations become important in the case of multiple simultaneous compounds or when the downstream metabolites of a drug are of interest. In the case of either multiple drugs or when there is a need to visualize both a compound and its delivery vehicle or formulation, fluorescent and Raman tools can still be used, but the potential interference between drug/compound contributions must be taken into consideration. For example, recent efforts visualizing the uptake of two fluorescent molecules would need to determine if their spectral or lifetime properties overlap. Similarly, in the case of Raman methods, an important early step would be to assess the chemical similarity between the two compounds. Fluorescence and Raman techniques, while potentially able to visualize a particular molecule, may not have the sensitivity or specificity to quantify a drug’s metabolites. For these types of experiments, mass spectrometry tools offer robust performance and can be used to follow many simultaneous molecular species.

The parameters of study also significantly impact the choice of toolkit. For example, if a compound of interest is thought to penetrate rapidly into skin in less than one or two minutes, it would be prudent to see if multiphoton fluorescence or coherent Raman imaging approaches can be adapted, as they both have high temporal resolution capabilities. The site of uptake is another major consideration: for studies of skin in visible areas, it can be challenging to obtain skin samples for *ex vivo* experiments. The study of acne drugs on the

face is a good example, where it is crucial to visualize and quantify the uptake of drugs to their target, but at the same time extremely difficult to obtain live, fresh facial skin from teenage patients. For such studies, non-invasive microscopy clinical imaging systems are good choices. Recent developments in creating microbiopsy tools that do not cause scarring may alleviate this problem in the near future [206-208]. Complex formulations, such as those found in many cosmetic products, also require special consideration, as they may contain numerous naturally-derived compounds that can interfere with fluorescence and Raman measurements. For these topical products, mass spectrometry approaches may be ideal.

The decision tree can also be driven by practical clinical considerations. For instance, mass spectrometry necessitates biopsies or excision of tissue samples from patients, which may not be possible in some cases. Autoradiography, while widely accepted in its use in preclinical and nonclinical studies, has significant safety concerns and regulatory barrier for use in human subjects, unless the diagnostic or therapeutic indication for use involves a radioactive compound. For Raman imaging, a deuterated compound may alter the pharmacokinetic behavior of the original molecule such that deuterated compounds may not be acceptable in some pharmaceutical or clinical development programs.

While the discussion has mostly centered on selecting a particular method for a given experiment, the methods discussed here can readily be combined to reveal otherwise unseen information. For instance, fluorescence and Raman techniques often make a natural pair; for example, a recent study examining the uptake and pharmacodynamic effects of sunfilter formulations observed the penetration of sunfilter compounds into deeper layers of the skin. Imaging of the carrier (Finsolv) with coherent Raman imaging revealed that the formulation was penetrating deep within skin, carrying the sunfilters with it [209]. Similarly, fluorescence imaging can be combined with mass spectrometry tools to glean both rapid temporal data *in vivo* and high content chemical information *ex vivo*. For example, fluorescence imaging can be used to follow a primary compound of interest in real-time, *in vivo*, in a clinical study. A biopsy acquired from the imaged site can later be interrogated with mass spectrometry to examine for compounds within the formulation, or perhaps for metabolites of that compound. While such a combination does not give simultaneous high temporal and chemical information, the combination of approaches can provide important information regarding the pharmacokinetics of the compound.

This combination of approaches is also important in the context of providing validation of a given method. MALDI mass spectrometry, for example, can be a sensitive method, but its sensitivity can be dependent on the ionization efficiency of a given molecule. Cross-validating a set of MALDI results with infrared or Raman imaging can provide an important check that results are correct and consistent. For methods such as coherent Raman, which have relatively low sensitivity, collecting tissue samples for secondary mass spectral analysis can be an important step in ensuring accurate compound quantification.

6. Conclusions

The tracking and quantification of drug and compound uptake into skin is critical for the pharmaceutical, cosmetic and environmental hazard testing fields. Small changes in environment, formulation, or chemical structure can have major effects on uptake, penetration, target engagement and clearing of molecular species in the skin. This review has offered a snapshot of current methods that can detect, identify, and quantify specific drugs or compounds within human skin. Ongoing research efforts, in the mass spectral and optical imaging fields in particular, continue to push the state-of-the-art in tissue chemical analysis. Numerous teams are pushing the speed, sensitivity, and portability of optical imaging tools to translate powerful chemical imaging modalities for non-invasive use on patients. Work in data science and machine learning are actively changing the way data is collected and analyzed, breaking down barriers and enabling quantitative analysis of otherwise unwieldly datasets [210]. Moreover, developments in user-friendly, ultrasensitive, compact, multimodal imaging systems and on-the-fly data analysis will drive forward the applications of these tools in human skin drug delivery. These translational research efforts promise to not only augment existing methods, but to change the paradigms of skin pharmacokinetic and pharmacodynamic measurements.

REFERENCES

[1]. Gregoire S, Luengo GS, Hallegot P, Pena AM, Chen X, Bornschlogl T, Chan KF, Pence I, Obeidy P, Feizpour A, Jeong S, Evans CL, Imaging and quantifying drug delivery in skin - Part 1: Autoradiography and mass spectrometry imaging, Adv Drug Deliv Rev, (2019).

[2]. Lakowicz JR, Principles of fluorescence spectroscopy, third ed., Springer, New York, 2006.

[3]. Yamada M, Tayeb H, Wang H, Dang N, Mohammed YH, Osseiran S, Belt PJ, Roberts MS, Evans CL, Sainsbury F, Prow TW, Using elongated microparticles to enhance tailorable nanoemulsion delivery in excised human skin and volunteers, J Control Release, 288 (2018) 264–276. [PubMed: 30227159]

[4]. Alex A, Frey S, Angelene H, Neitzel CD, Li J, Bower AJ, Spillman DR Jr., Marjanovic M, Chaney EJ, Medler JL, Lee W, Vasist Johnson LS, Boppart SA, Arp Z, In situ biodistribution and residency of a topical anti-inflammatory using fluorescence lifetime imaging microscopy, Br J Dermatol, 179 (2018) 1342–1350. [PubMed: 29989149]

[5]. Leite-Silva VR, Le Lamer M, Sanchez WY, Liu DC, Sanchez WH, Morrow I, Martin D, Silva HD, Prow TW, Grice JE, Roberts MS, The effect of formulation on the penetration of coated and uncoated zinc oxide nanoparticles into the viable epidermis of human skin in vivo, Eur J Pharm Biopharm, 84 (2013) 297–308. [PubMed: 23454052]

[6]. Lin LL, Grice JE, Butler MK, Zvyagin AV, Becker W, Robertson TA, Soyer HP, Roberts MS, Prow TW, Time-correlated single photon counting for simultaneous monitoring of zinc oxide nanoparticles and NAD(P)H in intact and barrier-disrupted volunteer skin, Pharm Res, 28 (2011) 2920–2930. [PubMed: 21717255]

[7]. Zvyagin AV, Zhao X, Gierden A, Sanchez W, Ross JA, Roberts MS, Imaging of zinc oxide nanoparticle penetration in human skin in vitro and in vivo, J Biomed Opt, 13 (2008) 064031. [PubMed: 19123677]

[8]. Mohammed YH, Holmes A, Haridass IN, Sanchez WY, Studier H, Grice JE, Benson HAE, Roberts MS, Support for the Safe Use of Zinc Oxide Nanoparticle Sunscreens: Lack of Skin Penetration or Cellular Toxicity after Repeated Application in Volunteers, J Invest Dermatol, 139 (2019) 308–315. [PubMed: 30448212]

[9]. Rawle CB, Lee CJ, Strachan CJ, Payne K, Manson PJ, Rades T, Towards characterization and identification of solid state pharmaceutical mixtures through second harmonic generation, J Pharm Sci, 95 (2006) 761–768. [PubMed: 16498571]

[10]. Strachan CJ, Rades T, Lee CJ, Determination of the optical second harmonic response of pharmaceutical solid-solid mixtures, Opt Laser Eng, 43 (2005) 209–220.

[11]. Prausnitz MR, Langer R, Transdermal drug delivery, Nat Biotechnol, 26 (2008) 1261–1268. [PubMed: 18997767]

[12]. Alkilani AZ, McCrudden MT, Donnelly RF, Transdermal Drug Delivery: Innovative Pharmaceutical Developments Based on Disruption of the Barrier Properties of the stratum corneum, Pharmaceutics, 7 (2015) 438–470. [PubMed: 26506371]

[13]. Sá GF, Serpa C, Arnaut LG, Stratum corneum permeabilization with photoacoustic waves generated by piezophotonic materials, J Control Release, 167 (2013) 290–300. [PubMed: 23419949]

[14]. Pawley JB, Handbook of biological confocal microscopy: Third edition, Springer US2006.

[15]. Sanderson MJ, Smith I, Parker I, Bootman MD, Fluorescence microscopy, Cold Spring Harb Protoc, 2014 (2014) pdb top071795.

[16]. Frombach J, Unbehauen M, Kurniasih IN, Schumacher F, Volz P, Hadam S, Rancan F, Blume-Peytavi U, Kleuser B, Haag R, Alexiev U, Vogt A, Core-multishell nanocarriers enhance drug penetration and reach keratinocytes and antigen-presenting cells in intact human skin, J Control Release, 299 (2019) 138–148. [PubMed: 30797867]

[17]. Volz P, Schilrreff P, Brodwolf R, Wolff C, Stellmacher J, Balke J, Morilla MJ, Zoschke C, Schäfer-Korting M, Alexiev U, Pitfalls in using fluorescence tagging of nanomaterials: Tectodendrimers in skin tissue as investigated by cluster-FLIM, Annals of the New York Academy of Sciences, Blackwell Publishing Inc., 2017, pp. 202–214.

[18]. Na R, Stender IM, Ma L, Wulf HC, Autofluorescence spectrum of skin: component bands and body site variations, Skin Res Technol, 6 (2000) 112–117. [PubMed: 11428953]

[19]. Fereidouni F, Bader AN, Colonna A, Gerritsen HC, Phasor analysis of multiphoton spectral images distinguishes autofluorescence components of in vivo human skin, J Biophotonics, 7 (2014) 589–596. [PubMed: 23576407]

[20]. Osseiran S, Roider EM, Wang H, Suita Y, Murphy M, Fisher DE, Evans CL, Non-Euclidean phasor analysis for quantification of oxidative stress in ex vivo human skin exposed to sun filters using fluorescence lifetime imaging microscopy, J Biomed Opt, 22 (2017) 1–10.

[21]. Masters BR, The Development of Fluorescence Microscopy, Encyclopedia of Life Sciences2010.

[22]. So PT, Dong CY, Masters BR, Berland KM, Two-photon excitation fluorescence microscopy, Annu Rev Biomed Eng, 2 (2000) 399–429. [PubMed: 11701518]

[23]. Jeong S, Hermsmeier M, Osseiran S, Yamamoto A, Nagavarapu U, Chan KF, Evans CL, Visualization of drug distribution of a topical minocycline gel in human facial skin, Biomed Opt Express, 9 (2018) 3434–3448. [PubMed: 29984108]

[24]. Hermsmeier M, Jeong S, Yamamoto A, Chen X, Nagavarapu U, Evans CL, Chan KF, Characterization of human cutaneous tissue autofluorescence: implications in topical drug delivery studies with fluorescence microscopy, Biomed Opt Express, 9 (2018) 5400–5418. [PubMed: 30460136]

[25]. Limon D, Fabrega MJ, Calpena AC, Badia J, Baldoma L, Perez-Garcia L, Multifunctional Serine Protease Inhibitor-Coated Water-Soluble Gold Nanoparticles as a Novel Targeted Approach for the Treatment of Inflammatory Skin Diseases, Bioconjug Chem, 29 (2018) 1060–1072. [PubMed: 29406699]

[26]. Alvarez-Roman R, Naik A, Kalia YN, Fessi H, Guy RH, Visualization of skin penetration using confocal laser scanning microscopy, Eur J Pharm Biopharm, 58 (2004) 301–316. [PubMed: 15296957]

[27]. Celli JP, Spring BQ, Rizvi I, Evans CL, Samkoe KS, Verma S, Pogue BW, Hasan T, Imaging and photodynamic therapy: mechanisms, monitoring, and optimization, Chem Rev, 110 (2010) 2795–2838. [PubMed: 20353192]

[28]. Rajadhyaksha M, Anderson RR, Webb RH, Video-rate confocal scanning laser microscope for imaging human tissues in vivo, Appl. Opt, 38 (1999) 2105–2115. [PubMed: 18319771]

[29]. Rajadhyaksha M, Gonzalez S, Zavislan JM, Anderson RR, Webb RH, In vivo confocal scanning laser microscopy of human skin II: advances in instrumentation and comparison with histology, J Invest Dermatol, 113 (1999) 293–303. [PubMed: 10469324]

[30]. Wilhelm K-P, Elsner P, Berardesca E, Maibach HI, Bioengineering of the Skin: Skin Imaging and Analysis, 2nd ed., Informa Healthcare USA, Inc.2007.

[31]. Freeman EE, Semeere A, Osman H, Peterson G, Rajadhyaksha M, Gonzalez S, Martin JN, Anderson RR, Tearney GJ, Kang D, Smartphone confocal microscopy for imaging cellular structures in human skin in vivo, Biomed Opt Express, 9 (2018) 1906–1915. [PubMed: 29675328]

[32]. Koehler MJ, Hahn S, Pieller A, Elsner P, Ziemer M, Bauer A, Konig K, Buckle R, Fluhr JW, Kaatz M, Morphological skin ageing criteria by multiphoton laser scanning tomography: non-invasive in vivo scoring of the dermal fibre network, Exp Dermatol, 17 (2008) 519–523. [PubMed: 18201192]

[33]. Koehler MJ, Preller A, Kindler N, Elsner P, Konig K, Buckle R, Kaatz M, Intrinsic, solar and sunbed-induced skin aging measured in vivo by multiphoton laser tomography and biophysical methods, Skin Res Technol, 15 (2009) 357–363. [PubMed: 19624433]

[34]. Kaatz M, Sturm A, Elsner P, Konig K, Buckle R, Koehler MJ, Depth-resolved measurement of the dermal matrix composition by multiphoton laser tomography, Skin Res Technol, 16 (2010) 131–136. [PubMed: 20456091]

[35]. Baldeweck T, Tancrède E, Dokladal P, Koudoro S, Morard V, Meyer F, Decencière E, Pena AM, *In vivo* multiphoton microscopy associated to 3D image processing for human skin characterization, Multiphoton Microscopy in the Biomedical Sciences XIISan Francisco, CA, 2012, pp. 82263o.

[36]. Koehler MJ, Preller A, Elsner P, Konig K, Hipler UC, Kaatz M, Non-invasive evaluation of dermal elastosis by in vivo multiphoton tomography with autofluorescence lifetime measurements, Exp Dermatol, 21 (2012) 48–51. [PubMed: 22151391]

[37]. Decencière E, Tancrède-Bohin E, Dokladal P, Koudoro S, Pena AM, Baldeweck T, Automatic 3D segmentation of multiphoton images: A key step for the quantification of human skin, Skin Res Technol, 19 (2013) 115–124. [PubMed: 23441573]

[38]. Sanchez WY, Obispo C, Ryan E, Grice JE, Roberts MS, Erratum: Changes in the redox state and endogenous fluorescence of in vivo human skin due to intrinsic and photo-aging, measured by multiphoton tomography with fluorescence lifetime imaging (Journal of Biomedical Optics (2013) 18 (061217)), J Biomed Opt, 18 (2013).

[39]. Miyamoto K, Kudoh H, Quantification and visualization of cellular NAD(P)H in young and aged female facial skin with in vivo two-photon tomography, Br J Dermatol, 169 Suppl 2 (2013) 25–31. [PubMed: 23786617]

[40]. Pena AM, Aguilar L, Azadiguian G, Baldeweck T, Baux L, Black A, Bornschlögl T, Brizion S, Chen X, Colonna A, Galey JB, Ngo B, Nouveau S, Rolland G, Sellathurai T, Sextius P, Tancrède-Bohin E, Tissot N, Victorin S, Multiphoton imaging in cosmetics research, in: Chan KF, Evans CL (Eds.) Visualizing and Quantifying Drug Distribution in Tissue III 2019, SPIE, San Franciso, California, USA, 2019, pp. 1085907.

[41]. Pena A-M, Decencière E, Brizion S, Koudoro S, Tancrède-Bohin E, Baldeweck T, In vivo 3D quantification of melanin in human skin based on multiphoton microscopy and image processing, 28th IFSCC Congress - International Federation of Societies of Cosmetic ChemistsParis, France, 2014, pp. 1129–1134.

[42]. König K, Speicher M, Bückle R, Reckfort J, McKenzie G, Welzel J, Koehler MJ, Elsner P, Kaatz M, Clinical optical coherence tomography combined with multiphoton tomography of patients with skin diseases, J Biophoton, 2 (2009) 389–397.

[43]. Dimitrow E, Riemann I, Ehlers A, Koehler MJ, Norgauer J, Elsner P, Konig K, Kaatz M, Spectral fluorescence lifetime detection and selective melanin imaging by multiphoton laser tomography for melanoma diagnosis, Exp Dermatol, 18 (2009) 509–515. [PubMed: 19243426]

[44]. Dimitrow E, Ziemer M, Koehler MJ, Norgauer J, Konig K, Elsner P, Kaatz M, Sensitivity and specificity of multiphoton laser tomography for *in vivo* and *ex vivo* diagnosis of malignant melanoma, J Invest Dermatol, 129 (2009) 1752–1758. [PubMed: 19177136]

[45]. Paoli J, Smedh M, Ericson MB, Multiphoton laser scanning microscopy--a novel diagnostic method for superficial skin cancers, Semin Cutan Med Surg, 28 (2009) 190–195. [PubMed: 19782943]

[46]. König K, Speicher M, Kohler MJ, Scharenberg R, Kaatz M, Clinical application of multiphoton tomography in combination with high-frequency ultrasound for evaluation of skin diseases, J Biophoton, 3 (2010) 759–773.

[47]. Koehler MJ, Speicher M, Lange-Asschenfeldt S, Stockfleth E, Metz S, Elsner P, Kaatz M, Konig K, Clinical application of multiphoton tomography in combination with confocal laser scanning microscopy for in vivo evaluation of skin diseases, Exp Dermatol, 20 (2011) 589–594. [PubMed: 21539618]

[48]. Seidenari S, Arginelli F, Dunsby C, French P, Konig K, Magnoni C, Manfredini M, Talbot C, Ponti G, Multiphoton laser tomography and fluorescence lifetime imaging of basal cell carcinoma: morphologic features for non-invasive diagnostics, Exp Dermatol, 21 (2012) 831–836. [PubMed: 22882324]

[49]. Seidenari S, Arginelli F, Bassoli S, Cautela J, Cesinaro AM, Guanti M, Guardoli D, Magnoni C, Manfredini M, Ponti G, Konig K, Diagnosis of BCC by multiphoton laser tomography, Skin Res Technol, 19 (2013) e297–304. [PubMed: 22776020]

[50]. Patalay R, Talbot C, Alexandrov Y, Lenz MO, Kumar S, Warren S, Munro I, Neil MA, Konig K, French PM, Chu A, Stamp GW, Dunsby C, Multiphoton multispectral fluorescence lifetime tomography for the evaluation of basal cell carcinomas, PLoS One, 7 (2012) e43460. [PubMed: 22984428]

[51]. Ulrich M, Klemp M, Darvin ME, Konig K, Lademann J, Meinke MC, In vivo detection of basal cell carcinoma: comparison of a reflectance confocal microscope and a multiphoton tomograph, J Biomed Opt, 18 (2013) 61229. [PubMed: 23456144]

[52]. Balu M, Kelly KM, Zachary CB, Harris RM, Krasieva TB, König K, Durkin AJ, Tromberg BJ, Distinguishing between benign and malignant melanocytic nevi by in vivo multiphoton microscopy, Cancer Research, 74 (2014) 2688–2697. [PubMed: 24686168]

[53]. Lentsch G, Balu M, Williams J, Lee S, Harris RM, Konig K, Ganesan A, Tromberg BJ, Nair N, Santhanam U, Misra M, In vivo multiphoton microscopy of melasma, Pigment Cell Melanoma Res, 32 (2019) 403–411. [PubMed: 30506627]

[54]. Huck V, Gorzelanny C, Thomas K, Getova V, Niemeyer V, Zens K, Unnerstall TR, Feger JS, Fallah MA, Metze D, Stander S, Luger TA, Koenig K, Mess C, Schneider SW, From morphology to biochemical state - intravital multiphoton fluorescence lifetime imaging of inflamed human skin, Sci Rep, 6 (2016) 22789. [PubMed: 27004454]

[55]. Lin J, Saknite I, Valdebran M, Balu M, Lentsch G, Williams JN, Koenig K, Tromberg BJ, Atanaskova Mesinkovska N, Feature characterization of scarring and non-scarring types of alopecia by multiphoton microscopy, Lasers Surg. Med, 51 (2019) 95–103. [PubMed: 30248187]

[56]. König K, Ehlers A, Stracke F, Riemann I, In vivo drug screening in human skin using femtosecond laser multiphoton tomography, Skin Pharmacol Physiol, 19 (2006) 78–88. [PubMed: 16685146]

[57]. Stracke F, Weiss B, Lehr CM, Konig K, Schaefer UF, Schneider M, Multiphoton microscopy for the investigation of dermal penetration of nanoparticle-borne drugs, J Invest Dermatol, 126 (2006) 2224–2233. [PubMed: 16710307]

[58]. Bazin R, Flament F, Colonna A, Le Harzic R, Buckle R, Piot B, Laize F, Kaatz M, Konig K, Fluhr JW, Clinical study on the effects of a cosmetic product on dermal extracellular matrix components using a high-resolution multiphoton tomograph, Skin Res Technol, 16 (2010) 305–310. [PubMed: 20636999]

[59]. König K, Raphael AP, Lin L, Grice JE, Soyer HP, Breunig HG, Roberts MS, Prow TW, Applications of multiphoton tomographs and femtosecond laser nanoprocessing microscopes in drug delivery research, Adv Drug Deliv Rev, 63 (2011) 388–404. [PubMed: 21514335]

[60]. Darvin ME, Konig K, Kellner-Hoefer M, Breunig HG, Werncke W, Meinke MC, Patzelt A, Sterry W, Lademann J, Safety assessment by multiphoton fluorescence/second harmonic generation/hyper-Rayleigh scattering tomography of ZnO nanoparticles used in cosmetic products, Skin Pharmacol Physiol, 25 (2012) 219–226. [PubMed: 22653438]

[61]. El Madani HA, Tancrede-Bohin E, Bensussan A, Colonna A, Dupuy A, Bagot M, Pena AM, *In vivo* multiphoton imaging of human skin: assessment of topical corticosteroid-induced epidermis atrophy and depigmentation, J Biomed Opt, 17 (2012) 026009. [PubMed: 22463041]

[62]. Darvin ME, Richter H, Ahlberg S, Haag SF, Meinke MC, Le Quintrec D, Doucet O, Lademann J, Influence of sun exposure on the cutaneous collagen/elastin fibers and carotenoids: Negative effects can be reduced by application of sunscreen, J Biophoton, 7 (2014) 735–743.

[63]. Tancrède-Bohin E, Baldeweck T, Decencière E, Brizion S, Victorin S, Parent N, Faugere J, Souverain L, Bagot M, Pena AM, Non-invasive short-term assessment of retinoids effects on human skin in vivo using multiphoton microscopy, J Eur Acad Dermatol Venereol, 29 (2015) 673–681. [PubMed: 25220296]

[64]. König K, Multiphoton Microscopy and Fluorescence Lifetime Imaging, Applications in Biology and Medicine, De Gruyter, Berlin, Boston, 2018.

[65]. Masters BR, So PT, Gratton E, Multiphoton excitation fluorescence microscopy and spectroscopy of *in vivo* human skin, Biophys J, 72 (1997) 2405–2412. [PubMed: 9168018]

[66]. Teuchner K, Freyer W, Leupold D, Volkmer A, Birch DJ, Altmeyer P, Stucker M, Hoffmann K, Femtosecond two-photon excited fluorescence of melanin, Photochem Photobiol, 70 (1999) 146–151. [PubMed: 10461455]

[67]. Campagnola PJ, Millard AC, Terasaki M, Hoppe PE, Malone CJ, Mohler WA, Three-dimensional high-resolution second-harmonic generation imaging of endogenous structural proteins in biological tissues, Biophys J, 82 (2002) 493–508. [PubMed: 11751336]

[68]. Zipfel WR, Williams RM, Christiet R, Nikitin AY, Hyman BT, Webb WW, Live tissue intrinsic emission microscopy using multiphoton-excited native fluorescence and second harmonic generation, Proc Natl Acad Sci U S A, 100 (2003) 7075–7080. [PubMed: 12756303]

[69]. König K, Riemann I, High-resolution multiphoton tomography of human skin with subcellular spatial resolution and picosecond time resolution, J Biomed Opt, 8 (2003) 432–439. [PubMed: 12880349]

[70]. Pena A, Strupler M, Boulesteix T, Schanne-Klein M, Spectroscopic analysis of keratin endogenous signal for skin multiphoton microscopy, Opt Express, 13 (2005) 6268–6274. [PubMed: 19498639]

[71]. Pena AM, Boulesteix T, Dartigalongue T, Schanne-Klein MC, Chiroptical effects in the second harmonic signal of collagens I and IV, J Am Chem Soc, 127 (2005) 10314–10322. [PubMed: 16028943]

[72]. Bancelin S, Aime C, Gusachenko I, Kowalczuk L, Latour G, Coradin T, Schanne-Klein MC, Determination of collagen fibril size via absolute measurements of second-harmonic generation signals, Nat Commun, 5 (2014) 4920. [PubMed: 25223385]

[73]. Göppert-Mayer M, Über Elementarakte mit zwei Quantensprüngen, Annalen der Physik, 401 (1931) 273–294.

[74]. Grzybowski A, Pietrzak K, Maria Goeppert-Mayer (1906-1972): two-photon effect on dermatology, Clin Dermatol, 31 (2013) 221–225. [PubMed: 23570069]

[75]. König K, Multiphoton microscopy in life sciences, Journal of Microscopy, 200 (2000) 83–104. [PubMed: 11106949]

[76]. Zipfel WR, Williams RM, Webb WW, Nonlinear magic: multiphoton microscopy in the biosciences, Nature Biotechnology, 21 (2003) 1369–1377.

[77]. Denk W, Strickler JH, Webb WW, Two-photon laser scanning fluorescence microscopy, Science, 248 (1990) 73–76. [PubMed: 2321027]

[78]. Grewal BS, Naik A, Irwin WJ, Gooris G, de Grauw CJ, Gerritsen HG, Bouwstra JA, Transdermal macromolecular delivery: real-time visualization of iontophoretic and chemically enhanced transport using two-photon excitation microscopy, Pharm Res, 17 (2000) 788–795. [PubMed: 10990196]

[79]. Yu B, Dong CY, So PT, Blankschtein D, Langer R, In vitro visualization and quantification of oleic acid induced changes in transdermal transport using two-photon fluorescence microscopy, J Invest Dermatol, 117 (2001) 16–25. [PubMed: 11442745]

[80]. Yu B, Kim KH, So PT, Blankschtein D, Langer R, Evaluation of fluorescent probe surface intensities as an indicator of transdermal permeant distributions using wide-area two-photon fluorescence microscopy, J Pharm Sci, 92 (2003) 2354–2365. [PubMed: 14603481]

[81]. Kushner J.t., Kim D, So PT, Blankschtein D, Langer RS, Dual-channel two-photon microscopy study of transdermal transport in skin treated with low-frequency ultrasound and a chemical enhancer, J Invest Dermatol, 127 (2007) 2832–2846. [PubMed: 17554365]

[82]. Lin CY, Lee GN, Jee SH, Dong CY, Lin SJ, Investigation of depilatory mechanism by use of multiphoton fluorescent microscopy, Confocal, Multiphoton, and Nonlinear Microscopic Imaging IIIMunich, 2007.

[83]. Luengo J, Weiss B, Schneider M, Ehlers A, Stracke F, Konig K, Kostka KH, Lehr CM, Schaefer UF, Influence of nanoencapsulation on human skin transport of flufenamic acid, Skin Pharmacol Physiol, 19 (2006) 190–197. [PubMed: 16679821]

[84]. Roberts MS, Roberts MJ, Robertson TA, Sanchez W, Thorling C, Zou Y, Zhao X, Becker W, Zvyagin AV, In vitro and in vivo imaging of xenobiotic transport in human skin and in the rat liver, J Biophotonics, 1 (2008) 478–493. [PubMed: 19343674]

[85]. Bender J, Simonsson C, Smedh M, Engstrom S, Ericson MB, Lipid cubic phases in topical drug delivery: visualization of skin distribution using two-photon microscopy, J Control Release, 129 (2008) 163–169. [PubMed: 18538886]

[86]. Lee JN, Jee SH, Chan CC, Lo W, Dong CY, Lin SJ, The effects of depilatory agents as penetration enhancers on human stratum corneum structures, J Invest Dermatol, 128 (2008) 2240–2247. [PubMed: 18401425]

[87]. Ahn J, Kim KH, Choe K, Lim JH, Lee SK, Kim YS, Kim P, Quantitative two-photon microscopy imaging analysis of human skin to evaluate enhanced transdermal delivery by hybrid-type multi-lamellar nanostructure, Biomed Opt Express, 9 (2018) 3974–3982. [PubMed: 30338168]

[88]. Geusens B, Van Gele M, Braat S, De Smedt SC, Stuart MCA, Prow TW, Sanchez W, Roberts MS, Sanders NN, Lambert J, Flexible nanosomes (SECosomes) enable efficient siRNA delivery in cultured primary skin cells and in the viable epidermis of ex vivo human skin, Ad Func Mater, 20 (2010) 4077–4090.

[89]. Labouta HI, Liu DC, Lin LL, Butler MK, Grice JE, Raphael AP, Kraus T, El-Khordagui LK, Soyer HP, Roberts MS, Schneider M, Prow TW, Gold nanoparticle penetration and reduced metabolism in human skin by toluene, Pharm Res, 28 (2011) 2931–2944. [PubMed: 21833791]

[90]. Leite-Silva VR, Lamer ML, Sanchez WY, Liu DC, Sanchez WH, Morrow I, Martin D, Silva HDT, Prow TW, Grice JE, Roberts MS, The effect of formulation on the penetration of coated and uncoated zinc oxide nanoparticles into the viable epidermis of human skin in vivo, Eur. J. Pharm. Biopharm, 84 (2013) 297–308. [PubMed: 23454052]

[91]. Belsey NA, Garrett NL, Contreras-Rojas LR, Pickup-Gerlaugh AJ, Price GJ, Moger J, Guy RH, Evaluation of drug delivery to intact and porated skin by coherent Raman scattering and fluorescence microscopies, J Control Release, 174 (2014) 37–42. [PubMed: 24231405]

[92]. Periasamy A, Clegg RM, FLIM microscopy in biology and medicine, 1st ed., Chapman and Hall/CRC, Taylor & Francis Group, Boca Raton, Florida, 2010.

[93]. Dancik Y, Favre A, Loy CJ, Zvyagin AV, Roberts MS, Errata: Use of multiphoton tomography and fluorescence lifetime imaging to investigate skin pigmentationin vivo, J Biomed Opt, 18 (2013) 029802.

[94]. Hermsmeier M, Jeong S, Yamamoto A, Chen X, Nagavarapu U, Evans CL, Chan KF, Characterization of human cutaneous tissue autofluorescence: implications in topical drug delivery studies with fluorescence microscopy, Biomed. Opt. Express, 9 (2018) 5400–5418. [PubMed: 30460136]

[95]. Digman MA, Caiolfa VR, Zamai M, Gratton E, The phasor approach to fluorescence lifetime imaging analysis, Biophys J, 94 (2008) L14–16. [PubMed: 17981902]

[96]. Huang N, Short M, Zhao J, Wang H, Lui H, Korbelik M, Zeng H, Full range characterization of the Raman spectra of organs in a murine model, Opt Express, 19 (2011) 22892–22909. [PubMed: 22109167]

[97]. Evans CL, Xie XS, Coherent anti-Stokes Raman scattering microscopy: chemical imaging for biology and medicine, Annu Rev. Anal. Chem, 1 (2008) 883–909.

[98]. Lu FK, Basu S, Igras V, Hoang MP, Ji M, Fu D, Holtom GR, Neel VA, Freudiger CW, Fisher DE, Xie XS, Label-free DNA imaging in vivo with stimulated Raman scattering microscopy, Proc Natl Acad Sci U S A, 112 (2015) 11624–11629. [PubMed: 26324899]

[99]. Herschel W Experiments on the Refrangibility of the Invisible Rays of the Sun, Philosophical Transactions, 90 (1800) 284–292.

[100]. Davies T, The history of near infrared spectroscopic analysis: Past, present and future "From sleeping technique to the morning star of spectroscopy", 26 (1998) 17–19.

[101]. White JR, Herschel and the Puzzle of Infrared, American Scientist, 100 (2012) 218–225.

[102]. Workman J, Weyer L, Practical Guide to Interpretive Near-Infrared Spectroscopy, CRC Press2007.

[103]. Chan KLA, Kazarian S, Attenuated total reflection Fourier-transform infrared (ATR-FTIR) imaging of tissues and live cells, 2015.

[104]. Severcan F, Haris PI, Vibrational Spectroscopy in Diagnosis and Screening, IOS Press2012.

[105]. Lindon JC, Tranter GE, Koppenaal D Encyclopedia of Spectroscopy and Spectrometry, Elsevier Science2016.

[106]. Diem M, Miljković M., š, Bird B, Chernenko T, Schubert J, Marcsisin E, Mazur A, Kingston E, Zuser E, Papamarkakis K, Laver N, Applications of Infrared and Raman Microspectroscopy of Cells and Tissue in Medical Diagnostics: Present Status and Future Promises %J Spectroscopy: An International Journal, 27 (2012) 34.

[107]. Bellisola G, Sorio C, Infrared spectroscopy and microscopy in cancer research and diagnosis, Am J Cancer Res, 2 (2012) 1–21. [PubMed: 22206042]

[108]. Bauer A, Hertzberg O, Kuderle A, Strobel D, Pleitez MA, Mantele W, IR-spectroscopy of skin in vivo: Optimal skin sites and properties for non-invasive glucose measurement by photoacoustic and photothermal spectroscopy, J Biophotonics, 11 (2018) e201600261.

[109]. Chalmers J, Griffiths P, Handbook of Vibrational Spectroscopy, 5 volumes set, Wiley2002.

[110]. Ioannidis JP, Castaldi P, Evangelou E, A compendium of genome-wide associations for cancer: critical synopsis and reappraisal, J Natl Cancer Inst, 102 (2010) 846–858. [PubMed: 20505153]

[111]. Chandra H, Reddy PJ, Srivastava S, Protein microarrays and novel detection platforms, Expert Rev Proteomics, 8 (2011) 61–79. [PubMed: 21329428]

[112]. Mendelsohn R, Flach CR, Moore DJ, Determination of molecular conformation and permeation in skin via IR spectroscopy, microscopy, and imaging, Biochim Biophys Acta, 1758 (2006) 923–933. [PubMed: 16730643]

[113]. Ongpipattanakul B, Francoeur ML, Potts RO, Polymorphism in stratum corneum lipids, Biochim Biophys Acta, 1190 (1994) 115–122. [PubMed: 8110804]

[114]. Potts RO, Francoeur ML, Lipid biophysics of water loss through the skin, Proc Natl Acad Sci U S A, 87 (1990) 3871–3873. [PubMed: 2339127]

[115]. Potts RO, Golden GM, Francoeur ML, Mak VH, Guy RH, Mechanism and enhancement of solute transport across the stratum corneum, J Control Release, 15 (1991) 249–260.

[116]. Potts RO, Guy RH, Francoeur ML, Routes of ionic permeability through mammalian skin, Solid State Ionics, 53 (1992) 165–169.

[117]. Tong PL, Roediger B, Kolesnikoff N, Biro M, Tay SS, Jain R, Shaw LE, Grimbaldeston MA, Weninger W, The skin immune atlas: three-dimensional analysis of cutaneous leukocyte subsets by multiphoton microscopy, J Invest Dermatol, 135 (2015) 84–93. [PubMed: 25007044]

[118]. Hong G, Antaris AL, Dai H, Near-infrared fluorophores for biomedical imaging, Nat Biomed Eng, 1 (2017) 0010.

[119]. Gurjarpadhye AA, Parekh MB, Dubnika A, Rajadas J, Inayathullah M, Infrared Imaging Tools for Diagnostic Applications in Dermatology, SM J Clin Med Imaging, 1 (2015) 1–5. [PubMed: 26691203]

[120]. Wrobel TP, Bhargava R, Infrared spectroscopic imaging advances as an analytical technology for biomedical sciences, Anal Chem, 90 (2017) 1444–1463.

[121]. Chalmers JM, Edwards HG, Hargreaves MD, Infrared and Raman spectroscopy in forensic science, John Wiley & Sons2012.

[122]. Zhang D, Wang H-J, Cui X-M, Wang C-X, Evaluations of imidazolium ionic liquids as novel skin permeation enhancers for drug transdermal delivery, Pharm Dev Technol, 22 (2017) 511–520. [PubMed: 26763663]

[123]. Marcott C, Lo M, Kjoller K, Domanov Y, Balooch G, Luengo GS, Nanoscale infrared (IR) spectroscopy and imaging of structural lipids in human stratum corneum using an atomic force microscope to directly detect absorbed light from a tunable IR laser source, Exp Dermatol, 22 (2013) 419–421. [PubMed: 23651342]

[124]. Gigler AM, Huber AJ, Bauer M, Ziegler A, Hillenbrand R, Stark RW, Nanoscale residual stress-field mapping around nanoindents in SiC by IR s-SNOM and confocal Raman microscopy, Opt Express, 17 (2009) 22351–22357. [PubMed: 20052158]

[125]. Balázs B, Sipos P, Danciu C, Avram S, Soica C, Dehelean C, Varju G, Erős G, Budai-Szűcs M, Berkó S, ATR-FTIR and Raman spectroscopic investigation of the electroporation-mediated transdermal delivery of a nanocarrier system containing an antitumour drug, Biomed. Opt. Express, 7 (2016) 67–78. [PubMed: 26819818]

[126]. Zhang Q, Saad P, Mao G, Walters RM, Mack Correa MC, Mendelsohn R, Flach CR, Infrared spectroscopic imaging tracks lateral distribution in human stratum corneum, Pharm Res, 31 (2014) 2762–2773. [PubMed: 24792828]

[127]. McAuley WJ, Chavda-Sitaram S, Mader KT, Tetteh J, Lane ME, Hadgraft J, The effects of esterified solvents on the diffusion of a model compound across human skin: an ATR-FTIR spectroscopic study, Int J Pharm, 447 (2013) 1–6. [PubMed: 23428880]

[128]. Wang K, Yan Y, Zhao G, Xu W, Dong K, You C, Zhang L, Xing J, In vitro and in vivo application of hydroxypropyl-β-cyclodextrin-grafted polyethyleneimine used as a transdermal penetration enhancer, Polym Chem, 5 (2014) 4658–4669.

[129]. Schwarz JC, Pagitsch E, Valenta C, Comparison of ATR–FTIR spectra of porcine vaginal and buccal mucosa with ear skin and penetration analysis of drug and vehicle components into pig ear, Eur J Pharm Sci, 50 (2013) 595–600. [PubMed: 23277290]

[130]. Bhargava R, Infrared spectroscopic imaging: the next generation, Appl Spectrosc, 66 (2012) 1091–1120. [PubMed: 23031693]

[131]. Lucassen GW, van Veen GN, Jansen JA, Band analysis of hydrated human skin stratum corneum attenuated total reflectance fourier transform infrared spectra in vivo, J Biomed Opt, 3 (1998) 267–280. [PubMed: 23015080]

[132]. Babita K, Kumar V, Rana V, Jain S, Tiwary AK, Thermotropic and spectroscopic behavior of skin: relationship with percutaneous permeation enhancement, Curr Drug Deliv, 3 (2006) 95–113. [PubMed: 16472099]

[133]. Pensack RD, Michniak BB, Moore DJ, Mendelsohn R, Infrared kinetic/structural studies of barrier reformation in intact stratum corneum following thermal perturbation, Appl Spectrosc, 60 (2006) 1399–1404. [PubMed: 17217589]

[134]. Boncheva M, Damien F, Normand V, Molecular organization of the lipid matrix in intact Stratum corneum using ATR-FTIR spectroscopy, Biochim Biophys Acta, 1778 (2008) 1344–1355. [PubMed: 18298945]

[135]. Bouwstra JA, Ponec M, The skin barrier in healthy and diseased state, Biochim Biophys Acta, 1758 (2006) 2080–2095. [PubMed: 16945325]

[136]. Karande P, Jain A, Ergun K, Kispersky V, Mitragotri S, Design principles of chemical penetration enhancers for transdermal drug delivery, 102 (2005) 4688–4693.

[137]. Xiao C, Moore DJ, Rerek ME, Flach CR, Mendelsohn R, Feasibility of tracking phospholipid permeation into skin using infrared and Raman microscopic imaging, J Invest Dermatol, 124 (2005) 622–632. [PubMed: 15737204]

[138]. Mendelsohn R, Chen H-C, Rerek M, Moore D, Infrared microspectroscopic imaging maps the spatial distribution of exogenous molecules in skin, 2003.

[139]. Nawaz A, Wong TW, Quantitative characterization of chitosan in the skin by Fourier-transform infrared spectroscopic imaging and ninhydrin assay: application in transdermal sciences, J Microsc, 263 (2016) 34–42. [PubMed: 26695532]

[140]. Pleitez MA, Hertzberg O, Bauer A, Lieblein T, Glasmacher M, Tholl H, Mantele W, Infrared reflectometry of skin: Analysis of backscattered light from different skin layers, Spectrochim Acta A Mol Biomol Spectrosc, 184 (2017) 220–227. [PubMed: 28500960]

[141]. Silbey RJ, Principles of Nonlinear Optical Spectroscopy By Shaul Mukamel (University of Rochester). Oxford University Press: New York 1995. xviii+ 543 pp. $65.00. ISBN 0-19-509278-3, ACS Publications, 1996.

[142]. Austin LA, Osseiran S, Evans CL, Raman technologies in cancer diagnostics, Analyst, 141 (2016) 476–503. [PubMed: 26539569]

[143]. Pence I, Mahadevan-Jansen A, Clinical instrumentation and applications of Raman spectroscopy, Chem Soc Rev, 45 (2016) 1958–1979. [PubMed: 26999370]

[144]. Caspers PJ, Lucassen GW, Bruining HA, Puppels GJ, Automated depth-scanning confocal Raman microspectrometer for rapid in vivo determination of water concentration profiles in human skin, J Raman Spectrosc, 31 (2000) 813–818.

[145]. Bonnist EY, Gorce JP, Mackay C, Pendlington RU, Pudney PD, Measuring the penetration of a skin sensitizer and its delivery vehicles simultaneously with confocal Raman spectroscopy, Skin Pharmacol Physiol, 24(2011) 274–283. [PubMed: 21701247]

[146]. Smith GP, McGoverin CM, Fraser SJ, Gordon KC, Raman imaging of drug delivery systems, Adv Drug Deliv Rev, 89 (2015) 21–41. [PubMed: 25632843]

[147]. Förster M, Bolzinger M-A, Ach D, Montagnac G, Briançon S. Ingredients tracking of cosmetic formulations in the skin: a confocal Raman microscopy investigation, Pharm Res, 28 (2011) 858–872. [PubMed: 21213026]

[148]. Tfayli A, Piot O, Pitre F, Manfait M, Follow-up of drug permeation through excised human skin with confocal Raman microspectroscopy, Eur Biophys J, 36 (2007) 1049–1058. [PubMed: 17565493]

[149]. Essendoubi M, Gobinet C, Reynaud R, Angiboust JF, Manfait M, Piot O, Human skin penetration of hyaluronic acid of different molecular weights as probed by Raman spectroscopy, Skin Res Technol, 22 (2016) 55–62. [PubMed: 25877232]

[150]. Franzen L, Anderski J, Planz V, Kostka KH, Windbergs M, Combining confocal R aman microscopy and freeze-drying for quantification of substance penetration into human skin, Exp Dermatol, 23 (2014) 942–944. [PubMed: 25219950]

[151]. Caspers PJ, Lucassen GW, Carter EA, Bruining HA, Puppels GJ, In vivo confocal Raman microspectroscopy of the skin: noninvasive determination of molecular concentration profiles, J Invest Dermatol, 116(2001) 434–442. [PubMed: 11231318]

[152]. Caspers PJ, Lucassen GW, Puppels GJ, Combined in vivo confocal Raman spectroscopy and confocal microscopy of human skin, Biophys J, 85 (2003) 572–580. [PubMed: 12829511]

[153]. Wang H, Zhang Q, Mao G, Conroy O, Pyatski Y, Fevola MJ, Cula GO, Maitra P, Mendelsohn R, Flach CR, Novel confocal Raman microscopy method to investigate hydration mechanisms in human skin, Skin Res Technol, 25 (2019) 653–661. [PubMed: 30932226]

[154]. Nakagawa N, Matsumoto M, Sakai S, In vivo measurement of the water content in the dermis by confocal Raman spectroscopy, Skin Res Technol, 16 (2010) 137–141. [PubMed: 20456092]

[155]. Pudney PD, Melot M, Caspers PJ, Van Der Pol A, Puppels GJ, An in vivo confocal Raman study of the delivery of trans retinol to the skin, Appl Spectrosc, 61 (2007) 804–811. [PubMed: 17716398]

[156]. Mélot M, Pudney PDA, Williamson A-M, Caspers PJ, Van Der Pol A, Puppels GJ, Studying the effectiveness of penetration enhancers to deliver retinol through the stratum comum by in vivo confocal Raman spectroscopy, J Control Release, 138 (2009) 32–39. [PubMed: 19401210]

[157]. Lademann J, Caspers PJ, Van Der Pol A, Richter H, Patzelt A, Zastrow L, Darvin M, Sterry W, Fluhr JW, In vivo Raman spectroscopy detects increased epidermal antioxidative potential with topically applied carotenoids, Laser Phys Lett, 6 (2009) 76–79.

[158]. Stamatas GN, de Sterke J, Hauser M, von Stetten O, van der Pol A, Lipid uptake and skin occlusion following topical application of oils on adult and infant skin, J Dermatol Sci, 50 (2008) 135–142. [PubMed: 18164596]

[159]. Choe C, Lademann J, Darvin ME, Confocal Raman microscopy for investigating the penetration of various oils into the human skin in vivo, J Derm Sci, 79 (2015) 176–178.

[160]. dos Santos L, Tippavajhala VK, Mendes TO, da Silva MGP, Fávero PP, Soto CAT, Martin AA, Evaluation of penetration process into young and elderly skin using confocal Raman spectroscopy, Vib Spectrosc, 100 (2019) 123–130.

[161]. Pot LM, Coenraads PJ, Blömeke B, Puppels GJ, Caspers PJ, Real-time detection of p-phenylenediamine penetration into human skin by in vivo R aman spectroscopy, Contact Dermatitis, 74 (2016) 152–158. [PubMed: 26778536]

[162]. dos Santos L, Sousa MPJ, Azoia NG, Cavaco-Paulo AM, Martin AA, Favero PP, In vivo confocal Raman spectroscopy and molecular dynamics analysis of penetration of retinyl acetate into stratum corneum, Spectrochimica Acta Part A: Molecular and Biomolecular Spectroscopy, 174 (2017) 279–285. [PubMed: 27960141]

[163]. Zhao J, Lui H, McLean DI, Zeng H, Integrated real-time Raman system for clinical in vivo skin analysis, Skin Res Technol, 14 (2008) 484–492. [PubMed: 18937786]

[164]. Franzen L, Selzer D, Fluhr JW, Schaefer UF, Windbergs M, Towards drug quantification in human skin with confocal Raman microscopy, Eur J Pharm Biopharm, 84 (2013) 437–444. [PubMed: 23220382]

[165]. Scotté C, de Aguiar HB, Marguet D, Green EM, Bouzy PVergnole S, Winlove CP, Stone N, Rigneault H, Assessment of compressive Raman versus hyperspectral Raman for microcalcification chemical imaging, Anal Chem, 90 (2018) 7197–7203. [PubMed: 29761698]

[166]. Réfrégier P, Scotté C, de Aguiar HB, Rigneault H, Galland F, Precision of proportion estimation with binary compressed Raman spectrum, JOSA A, 35 (2018) 125–134. [PubMed: 29328101]

[167]. Scotté C, Sivankutty S, Stockton P, Bartels RA, Rigneault H, Compressive Raman imaging with spatial frequency modulated illumination, Opt Lett, 44 (2019) 1936–1939. [PubMed: 30985779]

[168]. Soldevila F, Dong J, Tajahuerce E, Gigan S, de Aguiar HB, Fast compressive Raman bio-imaging via matrix completion, Optica, 6 (2019) 341–346.

[169]. Evans CL, Potma EO, Puoris'haag M, Cote D, Lin CP, Xie XS, Chemical imaging of tissue in vivo with video-rate coherent anti-Stokes Raman scattering microscopy, Proc Natl Acad Sci U S A, 102 (2005) 16807–16812. [PubMed: 16263923]

[170]. Evans CL, Xie XS, Coherent anti-stokes Raman scattering microscopy: chemical imaging for biology and medicine, Annu Rev Anal Chem, 1 (2008) 883–909.

[171]. Cheng J-X, Volkmer A, Xie XS, Theoretical and experimental characterization of coherent anti-Stokes Raman scattering microscopy, JOSA B, 19 (2002) 1363–1375.

[172]. Ganikhanov F, Evans CL, Saar BG, Xe XS, High-sensitivity vibrational imaging with frequency modulation coherent anti-Stokes Raman scattering (FM CARS) microscopy, Opt Lett, 31 (2006) 1872–1874. [PubMed: 16729099]

[173]. Cheng JX, Jia YK, Zheng G, Xie XS, Laser-scanning coherent anti-Stokes Raman scattering microscopy and applications to cell biology, Biophys J, 83 (2002) 502–509. [PubMed: 12080137]

[174]. Brinkmann M, Fast A, Hellwig T, Pence I, Evans CL, Fallnich C, Portable all-fiber dual-output widely tunable light source for coherent Raman imaging, Biomed. Opt. Express, (2019).

[175]. Kee TW, Cicerone MT, Simple approach to one-laser, broadband coherent anti-Stokes Raman scattering microscopy, Opt Lett, 29 (2004) 2701–2703. [PubMed: 15605477]

[176]. Ozeki Y, Umemura W, Sumimura K, Nishizawa N, Fukui K, Itoh K, Stimulated Raman hyperspectral imaging based on spectral filtering of broadband fiber laser pulses, Opt Lett, 37 (2012) 431–433. [PubMed: 22297376]

[177]. Zhang D, Wang P, Slipchenko MN, Ben-Amotz D, Weiner AM, Cheng JX, Quantitative vibrational imaging by hyperspectral stimulated Raman scattering microscopy and multivariate curve resolution analysis, Anal Chem, 85 (2013) 98–106. [PubMed: 23198914]

[178]. Figueroa B, Fu W, Nguyen T, Shin K, Manifold B, Wise F, Fu D, Broadband hyperspectral stimulated Raman scattering microscopy with a parabolic fiber amplifier source, Biomed Opt Express, 9 (2018) 6116–6131. [PubMed: 31065417]

[179]. Slipchenko MN, Le TT, Chen H, Cheng JX, High-speed vibrational imaging and spectral analysis of lipid bodies by compound Raman microscopy, J Phys Chem B, 113 (2009) 7681–7686. [PubMed: 19422201]

[180]. Yue S, Cardenas-Mora JM, Chaboub LS, Lelievre SA, Cheng JX, Label-free analysis of breast tissue polarity by Raman imaging of lipid phase, Biophys J, 102 (2012) 1215–1223. [PubMed: 22404944]

[181]. Galli R, Uckermann O, Winterhalder MJ, Sitoci-Ficici KH, Geiger KD, Koch E, Schackert G, Zumbusch A, Steiner G, Kirsch M, Vibrational spectroscopic imaging and multiphoton microscopy of spinal cord injury, Anal Chem, 84 (2012) 8707–8714. [PubMed: 22970705]

[182]. Rocha-Mendoza I, Langbein W, Borri P, Coherent anti-Stokes Raman microspectroscopy using spectral focusing with glass dispersion, Appl Phys Lett, 93 (2008) 201103.

[183]. Zhang D, Wang P, Slipchenko MN, Ben-Amotz D, Weiner AM, Cheng J-X, Quantitative vibrational imaging by hyperspectral stimulated Raman scattering microscopy and multivariate curve resolution analysis, Analytical chemistry, 85 (2012) 98–106. [PubMed: 23198914]

[184]. Evans CL, Xu X, Kesari S, Xie XS, Wong ST, Young GS, Chemically-selective imaging of brain structures with CARS microscopy, Opt Express, 15 (2007) 12076–12087. [PubMed: 19547572]

[185]. Fu D, Lu FK, Zhang X, Freudiger C, Pernik DR, Holtom G, Xie XS, Quantitative chemical imaging with multiplex stimulated Raman scattering microscopy, J Am Chem Soc, 134 (2012) 3623–3626. [PubMed: 22316340]

[186]. Xie XS, Yu J, Yang WY, Living cells as test tubes, Science, 312 (2006) 228–230. [PubMed: 16614211]

[187]. Hu F, Zeng C, Long R, Miao Y, Wei L, Xu Q, Min W, Supermultiplexed optical imaging and barcoding with engineered polyynes, Nat Methods, 15 (2018) 194–200. [PubMed: 29334378]

[188]. Tipping WJ, Lee M, Serrels A, Brunton VG, Hulme AN, Stimulated Raman scattering microscopy: an emerging tool for drug discovery, Chem Soc Rev, 45 (2016) 2075–2089. [PubMed: 26839248]

[189]. Moura CC, Bourdakos KN, Tare RS, Oreffo RO, Mahajan S, Live-imaging of Bioengineered Cartilage Tissue using Multimodal Non-linear Molecular Imaging, Sci Rep, 9 (2019) 5561. [PubMed: 30944358]

[190]. Chen X, Grégoire S, Formanek F, Galey J-B, Rigneault H, Quantitative 3D molecular cutaneous absorption in human skin using label free nonlinear microscopy, J Control Release, 200 (2015) 78–86. [PubMed: 25550155]

[191]. Sarri B, Chen X, Canonge R, Grégoire S, Formanek F, Galey J-B, Potter A, Bornschlögl T, Rigneault H, In vivo quantitative molecular absorption of glycerol in human skin using coherent anti-Stokes Raman scattering (CARS) and two-photon auto-fluorescence, J Control Release, (2019).

[192]. Freudiger CW, Min W, Saar BG, Lu S Holtom GR, He C, Tsai JC, Kang JX, Xie XS, Label-free biomedical imaging with high sensitivity by stimulated Raman scattering microscopy, Science, 322 (2008) 1857–1861. [PubMed: 19095943]

[193]. Saar BG, Contreras-Rojas LR, Xie XS, Guy RH, Imaging drug delivery to skin with stimulated Raman scattering microscopy, Mol Pharm, 8 (2011) 969–975. [PubMed: 21548600]

[194]. Wei L, Hu F, Shen Y, Chen Z, Yu Y, Lin CC, Wang MC, Min W, Live-cell imaging of alkyne-tagged small biomolecules by stimulated Raman scattering, Nat Methods, 11 (2014) 410–412. [PubMed: 24584195]

[195]. Feizpour A, Bastholm L, Marstrand TT, Evans CL, Label-free Quantification of Pharmacokinetics in Skin, Bio-Optics: Design and Application, Optical Society of America, 2019, pp. JW3C. 1.

[196]. Ronneberger O, Fischer P, Brox T, U-net: Convolutional networks for biomedical image segmentation, International Conference on Medical image computing and computer-assisted intervention, Springer, 2015, pp. 234–241.

[197]. Potma EO, Evans CL, Xie XS, Heterodyne coherent anti-Stokes Raman scattering (CARS) imaging, Opt Lett, 31 (2006) 241–243. [PubMed: 16441043]

[198]. Evans CL, Potma EO, Xie XS, Coherent anti-stokes raman scattering spectral interferometry: determination of the real and imaginary components of nonlinear susceptibility chi(3) for vibrational microscopy, Opt Lett, 29 (2004) 2923–2925. [PubMed: 15645825]

[199]. Alexiev U, Volz P, Boreham A, Brodwolf R, Time-resolved fluorescence microscopy (FLIM) as an analytical tool in skin nanomedicine, Eur J Pharm Biopharm, 116 (2017) 111–124. [PubMed: 28115230]

[200]. Depieri LV, Praca FS, Campos PM, Bentley MV, Advances in the bioanalytical study of drug delivery across the skin, Ther Deliv, 6 (2015) 571–594. [PubMed: 26001174]

[201]. Pancholi K, A review of imaging methods for measuring drug release at nanometre scale: a case for drug delivery systems, Expert Opin Drug Deliv, 9 (2012) 203–218. [PubMed: 22235965]

[202]. Pappinen S, Pryazhnikov E, Khiroug L, Ericson MB, Yliperttula M, Urtti A, Organotypic cell cultures and two-photon imaging: tools for in vitro and in vivo assessment of percutaneous drug delivery and skin toxicity, J Control Release, 161 (2012) 656–667. [PubMed: 22465394]

[203]. Roberts MS, Dancik Y, Prow TW, Thorling CA, Lin LL, Grice JE, Robertson TA, Konig K, Becker W, Non-invasive imaging of skin physiology and percutaneous penetration using fluorescence spectral and lifetime imaging with multiphoton and confocal microscopy, Eur J Pharm Biopharm, 77 (2011) 469–488. [PubMed: 21256962]

[204]. König K, Raphael AP, Lin L, Grice JE, Soyer HP, Breunig HG, Roberts MS, Prow TW, Applications of multiphoton tomographs and femtosecond laser nanoprocessing microscopes in drug delivery research, Adv. Drug Del. Rev, 63 (2011) 388–404.

[205]. Tsai TH, Jee SH, Dong CY, Lin SJ, Multiphoton microscopy in dermatological imaging, J Dermatol Sci, 56 (2009) 1–8. [PubMed: 19699614]

[206]. Banan P, Lin LL, Lambie D, Prow T, Soyer HP, Effects of ex vivo skin microbiopsy on histopathologic diagnosis in melanocytic skin lesions, JAMA Dermatol, 149 (2013) 1107–1109. [PubMed: 23864191]

[207]. Lin LL, Prow TW, Raphael AP, Harrold Iii RL, Primiero CA, Ansaldo AB, Soyer HP, Microbiopsy engineered for minimally invasive and suture-free sub-millimetre skin sampling, F1000Res, 2 (2013) 120. [PubMed: 24627782]

[208]. Sobarun P, Hoang VL, Yamada M, Lambie D, Soyer HP, Prow TW, Microbiopsy Biomarker Profiling in a Superficial Melanoma Resembling a Pigmented Basal Cell Carcinoma, JAMA Dermatol, 153 (2017) 334–336. [PubMed: 28196220]

[209]. Osseiran S, Roider EM, Wang H, Suita Y, Murphy M, Fisher DE, Evans CL, Non-Euclidean phasor analysis for quantification of oxidative stress in ex vivo human skin exposed to sun filters using fluorescence lifetime imaging microscopy, Journal of biomedical optics, 22 (2017) 125004.

[210]. Gonzalez G, Evans CL, Biomedical Image Processing with Containers and Deep Learning: An Automated Analysis Pipeline: Data architecture, artificial intelligence, automated processing, containerization, and clusters orchestration ease the transition from data acquisition to insights in medium-to-large datasets, Bioessays, 41 (2019) e1900004. [PubMed: 31094000]

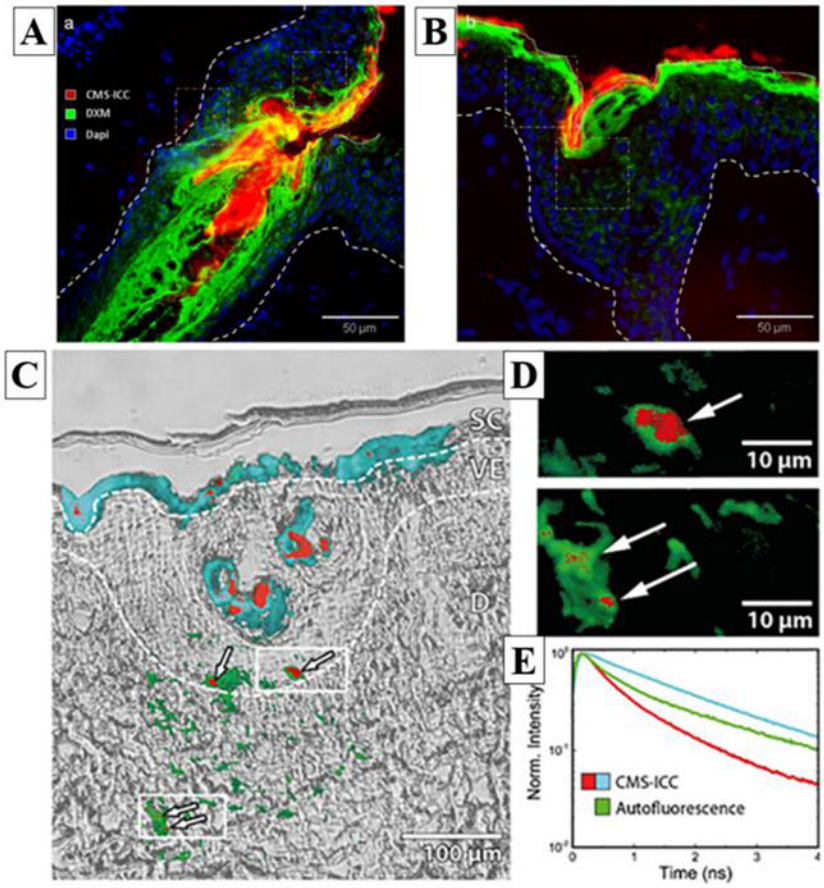

Figure 1.

Example of conventional fluorescence, FLIM and transmitted light images of a drug (DXM) and its core-multishell nanocarrier (CMS-NC) distributions within *ex vivo* human skin. A / B) conventional fluorescence images highlighting in red the nanocarrier CMS-ICC (indocarbocyanine-labelled CMS-NC), in green the DXM drug (anti-DXM primary-antibody coupled with Fluorescein isothiocyanate (FITC)-labelled secondary-antibody) and in blue the cells nuclei (DAPI staining); C) Transmitted light and conventional FLIM overlay images of CMS-ICC penetration in the skin section. Pseudo-colored fluorescence decay signatures shown in (E) indicate the localization of the CMS-ICC-NC; dashed lines indicate borders between *stratum corneum*, living epidermis and dermis layers. (D) Cluster-FLIM images of epidermal and dermal ICC-CMS-NC locations; zoom into regions of (C) as indicated by white rectangles. (E) Fluorescence decay signatures (ICC-CMS-NC: red, cyan; Autofluorescence: green) revealed by cluster-FLIM analysis. Reprinted from J. Control. Release, 299, Frombach *et al.*, Core-multishell nanocarriers enhance drug penetration and reach keratinocytes and antigen-presenting cells in intact human skin, 138-148, Copyright (2019), with permission from Elsevier [16].

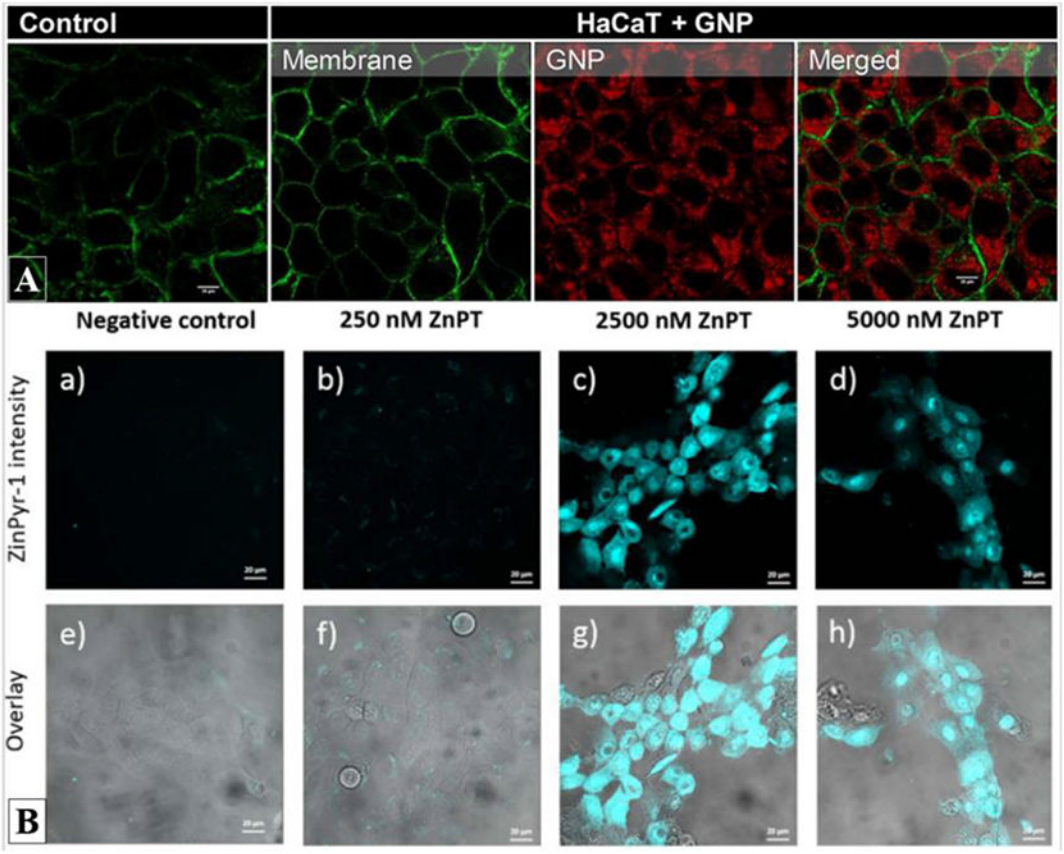

Figure 2.

Example of confocal fluorescence images of compound uptake within human keratinocytes. A) Internalization of BODIPY-labeled gold nanoparticles (red) into the cytoplasm of HaCaT keratinocytes stained with Alexa Fluor 488-conjugated with fluorescent wheat germ agglutinin (WGA) for glycocalyx membrane identification. Adapted with permission from Limon *et al.* Bioconjugate Chem. 29, 1060–1072 (2018) [25]. Copyright (2019) American Chemical Society; B) (top) Confocal fluorescence images of exogenous labelvZynPyr-1 (cyan) highlighting the intracellular labile zinc and its increase after application of different concentrations of zinc pyrithione (ZnPT) on HaCaT keratinocytes. (bottom) Overlay of confocal fluorescence and transmitted light images allowing to map the fluorophore's distribution within the cells. Reprinted from Toxicol. Appl. Pharmacol. 343, Holmes *et al.*, Imaging the penetration and distribution of zinc and zinc species after topical application of zinc pyrithione to human skin, 40-47, Copyright (2018), with permission from Elsevier [8].

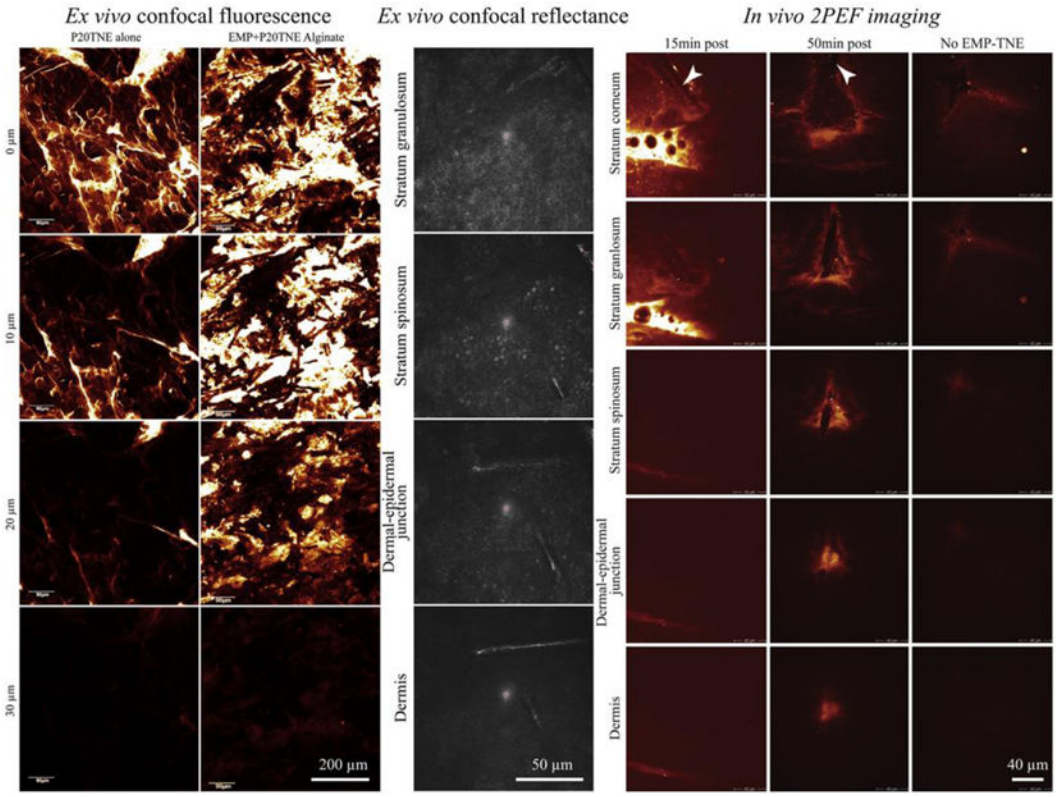

Figure 3.

Example of *ex vivo* confocal fluorescence, *in vivo* confocal reflectance and *in vivo* two-photon excited fluorescence images of elongated microparticles (EMP) combined with tailorable nanoemulsions (P20TNE) to alliance topical delivery of hydrophobic drug surrogates in human skin. (left) *ex vivo* confocal fluorescence images showing the distribution of a fluorescent lipophilic dye (DiI, incorporated within TNE) at the surface (0 μm), 10, 20 and 30 μm deep in human skin. The P20TNE alone appears to partition in the *stratum corneum* and furrows, whereas EMP coated with P20TNE using alginate (EMP +P20TNE Alginate) were capable of delivering detectable DiI around the dermal-epidermal junction at >30 μm deep. (middle) *Ex vivo* confocal reflectance images showing the presence of EMP+P20TNE Alginate through the excised living abdominal skin. (right) *In vivo* 2PEF images of human forearm skin after topical application TNE (alone and EMP +P20TNE Alginate) containing 6-Carboxyfluorescein (CaF) in the core droplet of the TNE. At 15 min post application, majority of TNE stayed at the surface of the skin, whereas at 50 min, more intense TNE signal released from EMP was detected at dermal-epidermal junction. Adapted from J. Control. Release, 288, Yamada *et al.* Using elongated microparticles to enhance tailorable nanoemulsion delivery in excised human skin and volunteers, 264-276, Copyright (2018), with permission from Elsevier [3].

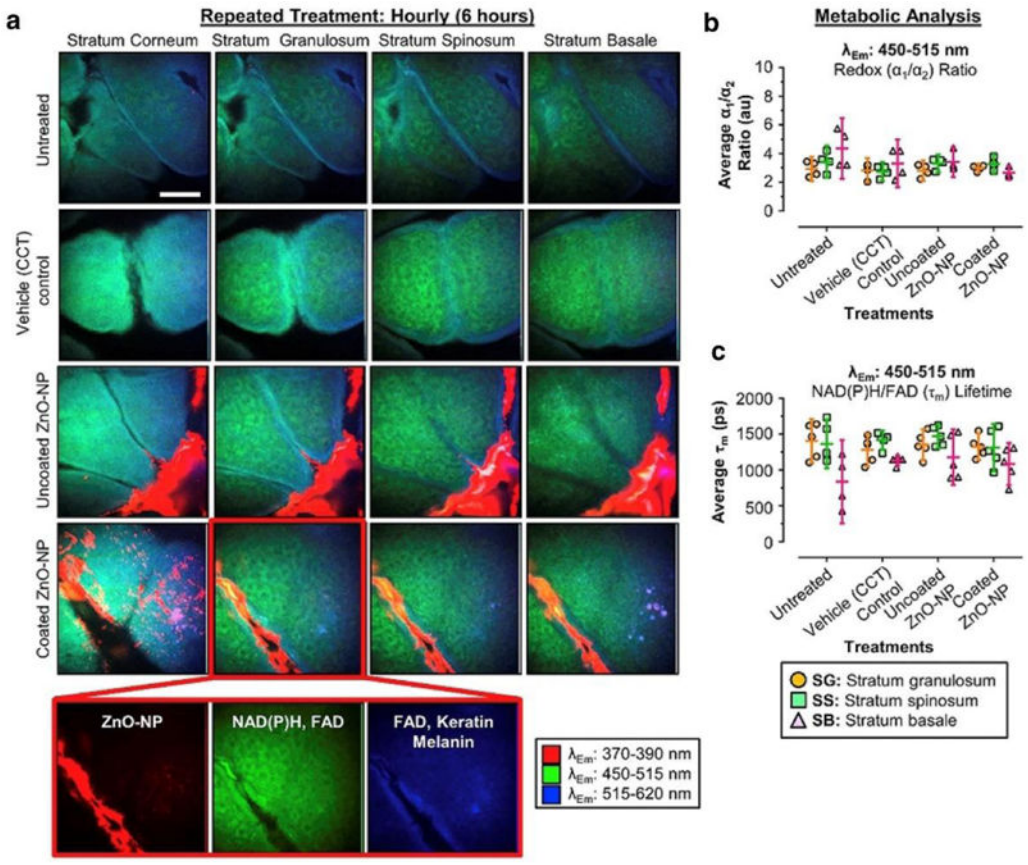

Figure 4.

Example of SHG application to *in vivo* human forearm skin drug delivery - effect of daily application of uncoated and coated ZnO-NPs on human skin *in vivo* for 5 days. Negative and vehicle controls are included. (a) Representative pseudocolored multispectral images (λ_{Em} =370-390 nm [red], λ_{Em} =450-515 mn [green], λ_{Em} =515-620 nm [blue] of different skin strata after treatment. The images were pseudocolored to show cellular autofluorescence (green/blue) and ZnO-NP (red). (b, c) Metabolic- and redox-associated changes in FLIM channel 2 (λ_{Em} =450-515 nm) in *stratum granulosum, stratum spinosum*, and *stratum basale* after treatment. (b) Average redox (α_1: α_2) ratios obtained after treatment. (c) Average fluorescence NAD(P)H/FAD lifetime (λ_{Em}) obtained after treatment. Data represent mean lifetime (ps) or ratio ± 95% confidence interval (n=5). Scale bar 40 μm. Em, emission; FAD, Flavin adenine dinucleotide; FLIM, fluorescence lifetime imaging microscopy; NAD(P)H, reduced nicotinamide adenine dinucleotide phosphate; NP, nanoparticle; ZnO, zinc oxide. Reprinted from J. Invest. Dermatol. 139/2, Mohammed *et al.* Support for the Safe Use of Zinc Oxide Nanoparticle Sunscreens: Lack of Skin Penetration or Cellular Toxicity after Repeated Application in Volunteers, 308-315, Copyright (2019), with permission from Elsevier [8].

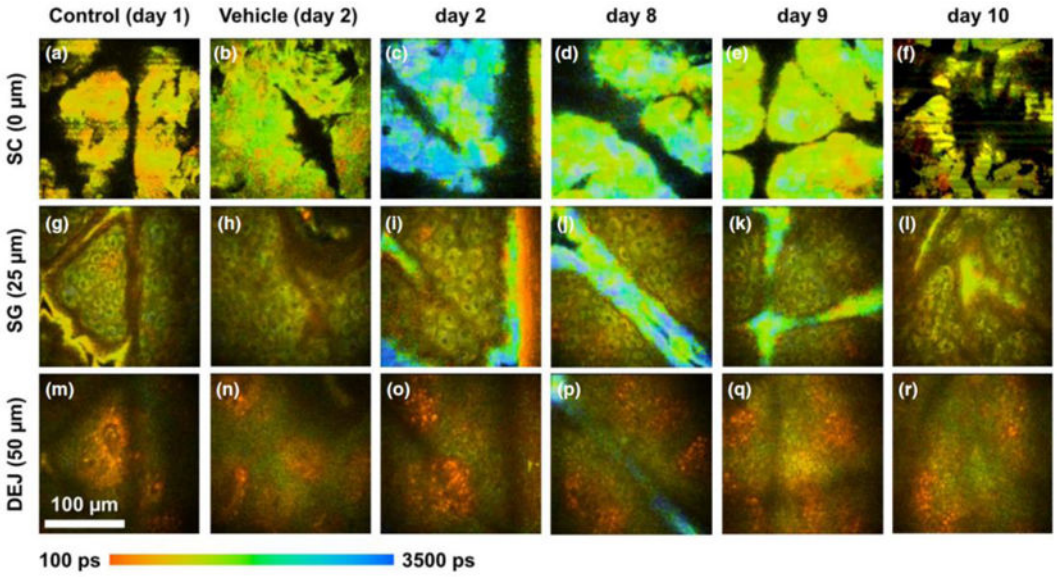

Figure 5.

Example of *in vivo* 2PEF-FLIM data obtained with bi-exponential fit analysis to assess the distribution and residency of a topically applied fluorescent cream on human forearm skin. All blue regions with longer fluorescence lifetime indicate signal from the fluorescent drug. The FLIM images were acquired daily throughout the study and at three different skin depths: (a–f) *stratum corneum* (SC), (g–1) *stratum granulosum* (SG) and (m–r) dermal–epidermal junction (DEJ). On treatment days 2–7, most of the drug signal was detected on the skin surface (c, d). Accumulation of the topical formulation along skin ridges is also visible in images obtained on days 2, 8 and 9 (i, j, k, p). By day 10, there was no detectable fluorescence from formulation residing in the skin (f, l, r). Reprinted from with permission from [4].

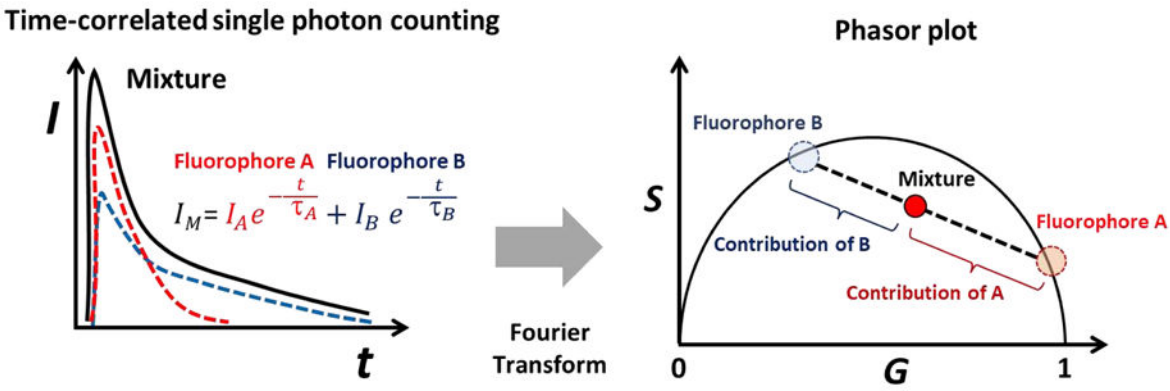

Figure 6.

Phasor analysis of two single lifetimes components τ_A and τ_B. Schematic of time-correlated single-photon counting fluorescence lifetime exponential decay traces (left) and the phasor plots of two fluorophores and their mixture (right). The contributions of two fluorophores to the mixture pixels can be determined by computing the distance between the pixel's phasor and two references phasor cluster.

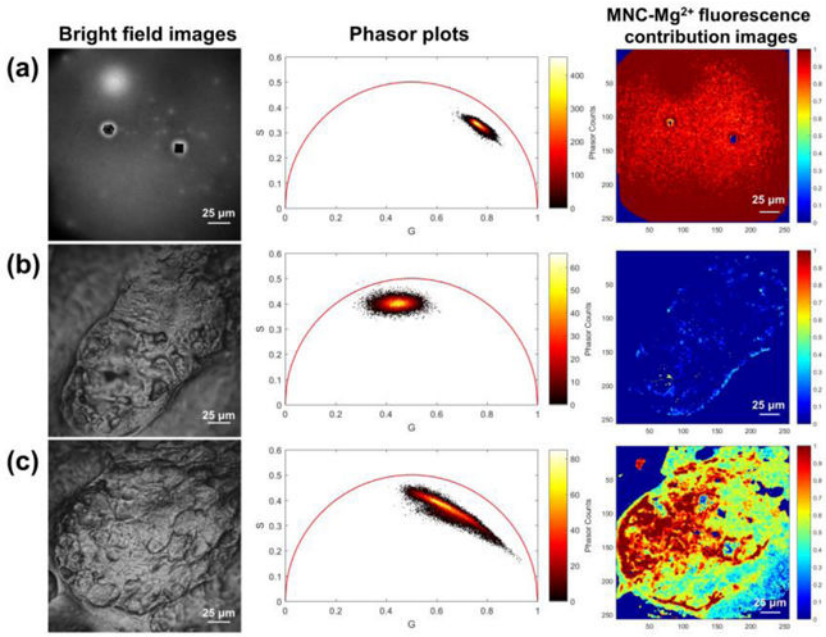

Figure 7.

Example of *ex vivo* 2PEF-FLIM data obtained with phasor analysis to assess the topically applied fluorescent drug within human facial skin. Bright field images, phasor plots, and MNC-Mg^{2+} fluorescence contribution images of (a) dried MNC-Mg^{2+}, (b) untreated sebaceous gland, and (c) sebaceous gland treated with MNC-Mg^{2+}. The phasor plots and MNC-Mg^{2+} fluorescence contribution images were generated from the red fluorescence channel (590-650 nm) using a non-Euclidean phasor analysis algorithm developed in Matlab [20]. All FLIM images were obtained with 90 s acquisition time. Reprinted with permission from Biomed. Opt. Express, 9, 3434-3448, 2018, Jeong *et al.* Visualization of drug distribution of a topical minocycline gel in human facial skin, ©Optical Society of America [23].

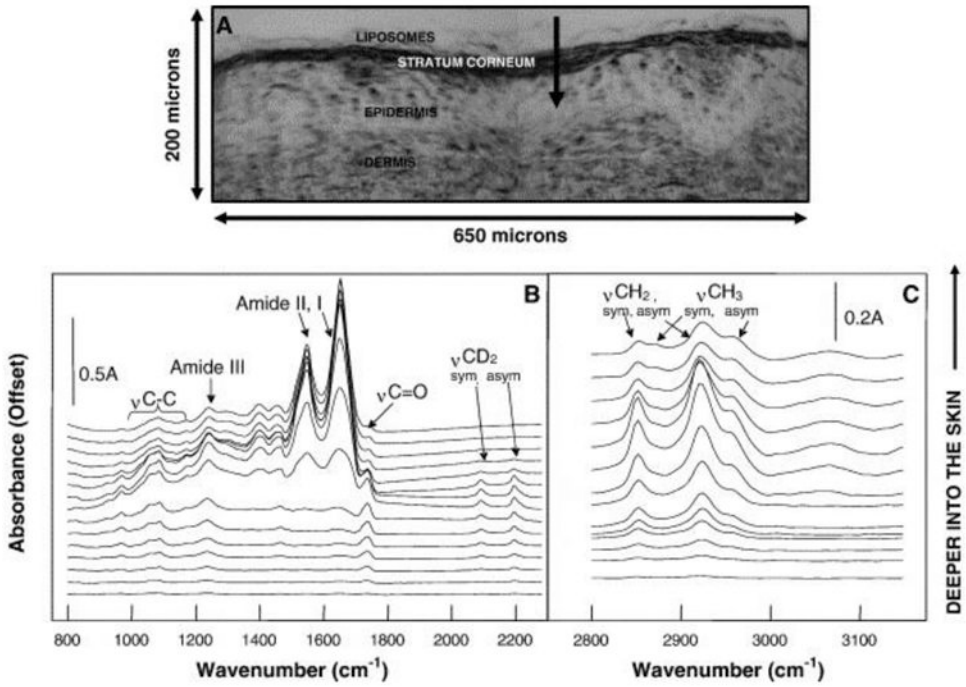

Figure 8.

IR spectroscopy for drug delivery in skin. A) Histological section of unstained pig skin where deuterated phospholipids were topically applied before imaging. The outer dark line shows the *stratum corneum*, the arrow starts in the topically applied formulation and goes towards the dermal layers of the skin. IR spectra recorded along the arrow (superficial spectra depicted at bottom) are shown in B) and C). For spectra close to the tip of the arrow (upper spectra) the typical skin signature becomes visible with strong Amide I and II vibrations from keratin, while the prior spectra obtained on the surface of the skin exhibit signal from the symmetric and asymmetric stretching CD_2 modes from the exogenous P-d_{31}OPC liposomes at approx. 2090 and 2190 cm^{-1}. Reprinted with permission from [112].

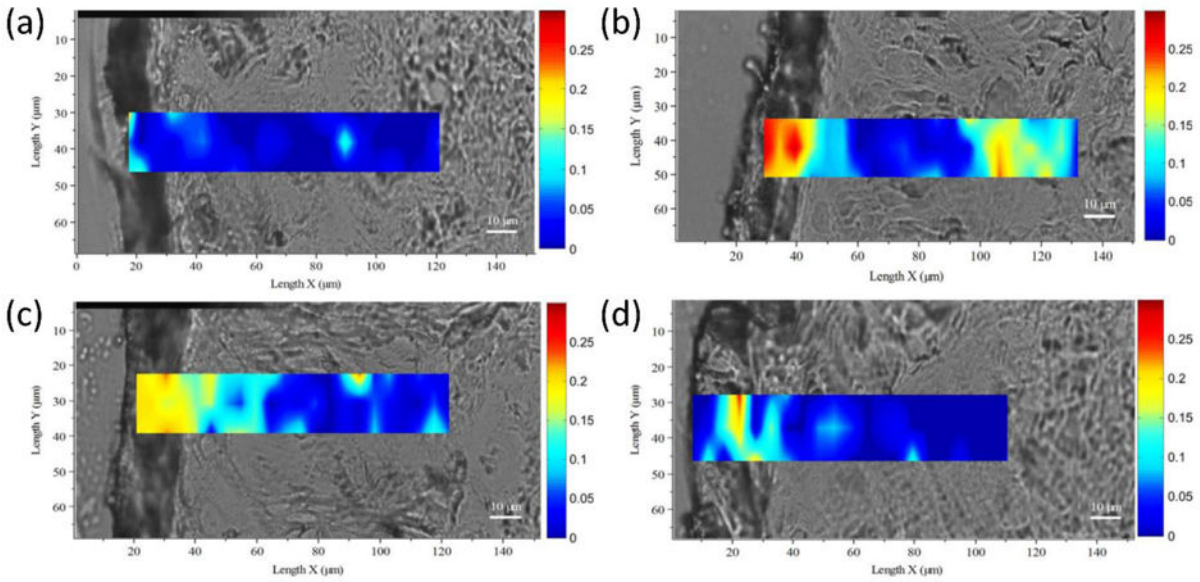

Figure 9.

Permeation and localization of various hyaluronic acid (b) Renovhyal (20-50 kDa HA), (c) Bashyal (100–300 kDa HA) and (d) Cristalhyal (1000–1400 kDa HA) in skin, in comparison with the control (a) water treated skin. Reprinted with permission from [149]

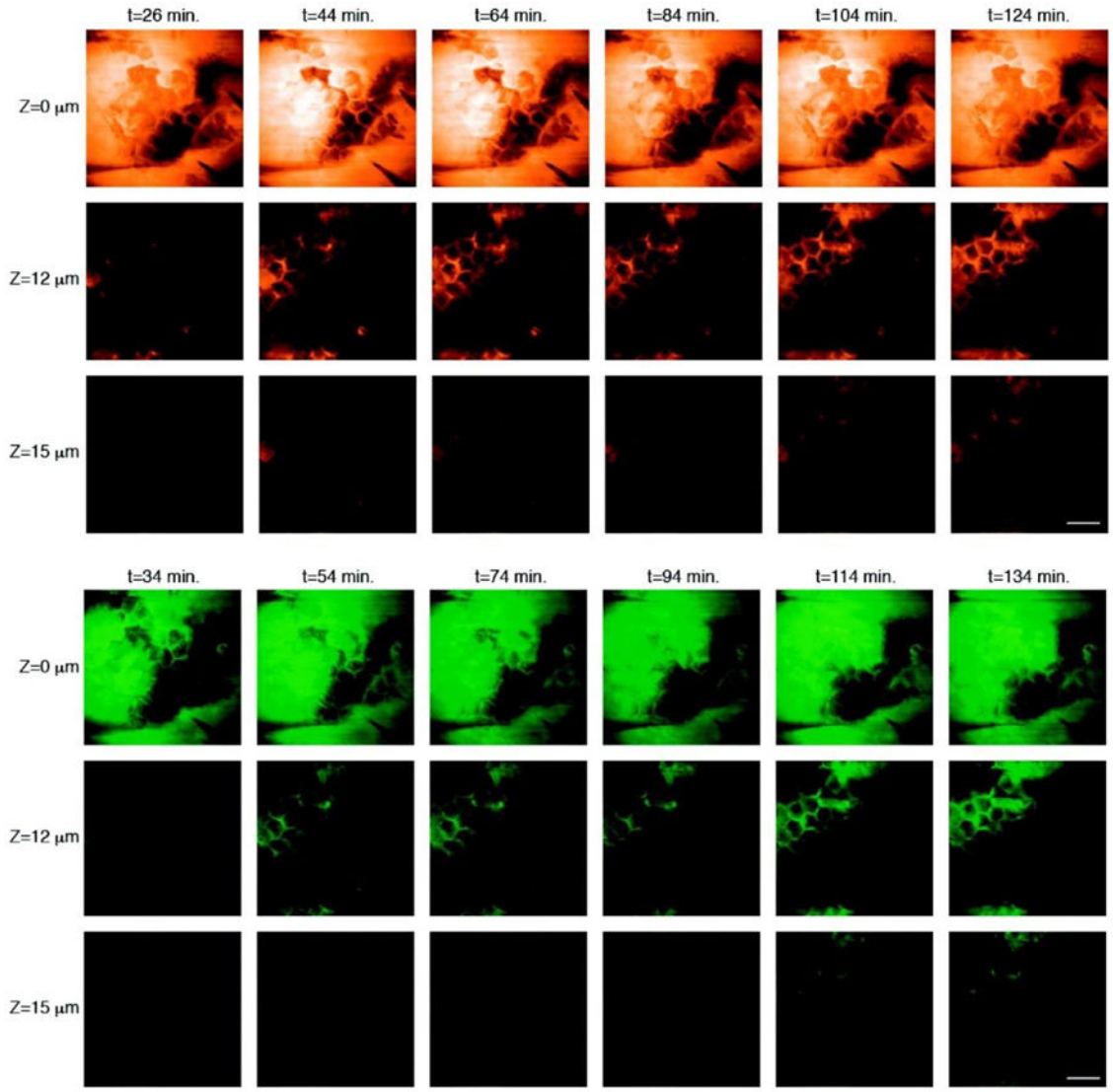

Figure 10.

Imaging the penetration of deuterated PG (upper panel) and ketoprofen (lower panel) across the stratum corneum. Images acquired at the depths indicated down the left-hand side of the figure and times indicated along the top show the penetration of cosolvait and drug into the tissue using SRS contrast at 2120 cm^{-1} and 1599 cm^{-1}, respectively. Scale bar = 50 μm. Reprinted with permission from Brian *et al.* Imaging Drug Delivery to Skin with Stimulated Raman Scattering Microscopy, Molecular Pharmaceutics 2011 8 (3), 969-975, DOI: 10.1021/mp200122w. Copyright 2011 American Chemical Society [193].

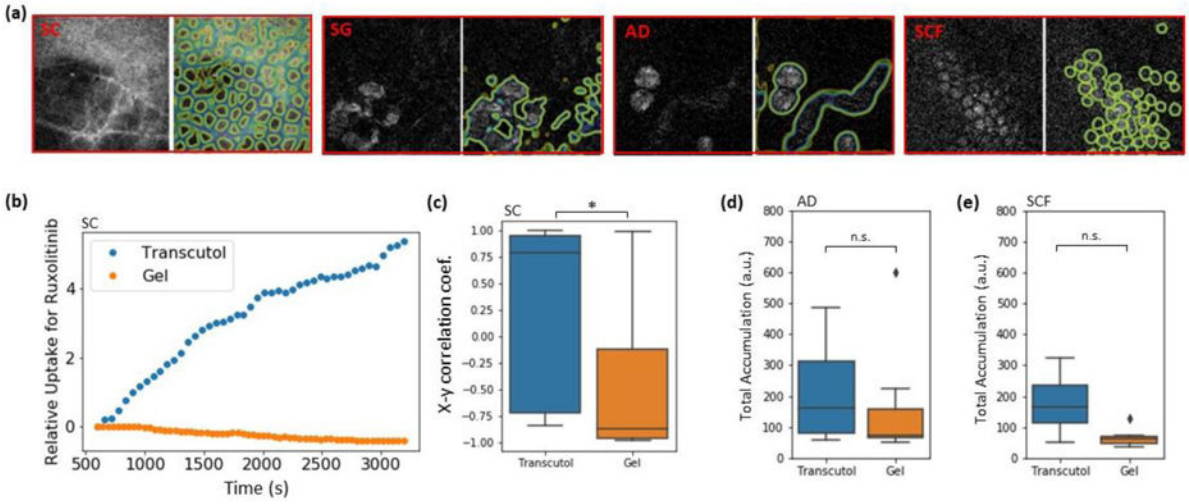

Figure 11.

(a) SRS images of SC, SG, AD and SCF layers in mouse epidermis (on the left side of each red box) and segmentation of the lipid-rich areas using 4 in-house-trained U-Net algorithms (on the right side of each red box). **(b)** Relative uptake of ruxolitinib over time in transcutol and a gel formulation in the lipid-rich regions of an SC image. **(c)** Pearson's correlation coefficient for 10 uptake patterns similar to what is shown in (a) for both ruxolitinib and BMDP-D in transcutol and gel showing a statistically significant difference between the two vehicles. ($p < 0.05$). **(d, e)** AUC calculated for the same experiments as in (c) but for the AD and SCF shows a non-significant difference between the two vehicles. Taken from [195] with permission.

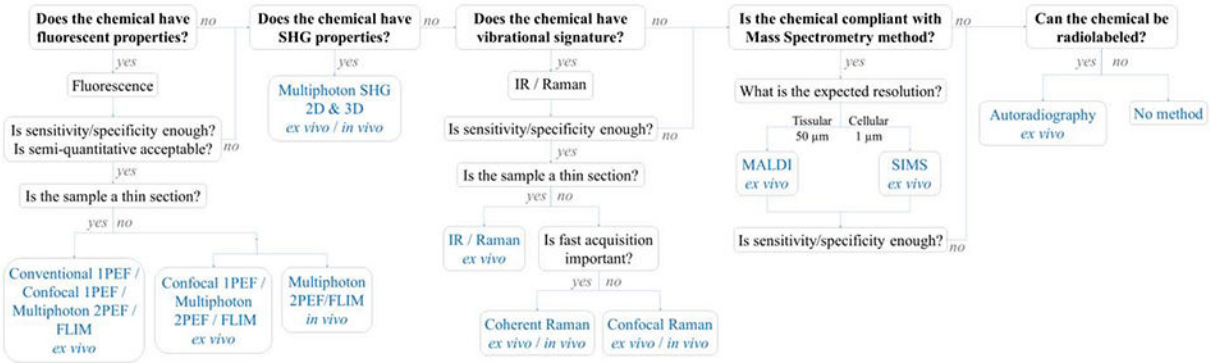

Figure 12.

Decision tree for selection of technique for quantitative imaging and analysis of drug delivery in skin.

Table 1:

Comparison of imaging methods

	Chemical	Specificity	Sensitivity	Temporal Resolution	Imaging Depth	Semi-/ Quantitative	Spatial resolution
Conventional / Confocal Fluorescence (1PEF)	Fluorophores, endogenous and exogenous	+	+++	+++	+	Semi quantitative	Subcellular (200 nm)
Multiphoton Fluorescence (2PEF / FLIM) and SHG	Fluorophores, endogenous and exogenous; special molecules	+	+++	+++	+++	Semi quantitative	Subcellular (300 nm)
Infrared Imaging	Any via spectroscopic fingerprints	+++	++	N/A	N/A	Quantitative	Cellular (1 μm)
Confocal Raman	Any via spectroscopic fingerprints	+++	++	+	+	Quantitative	Subcellular (300 nm)
Coherent Raman	Unique bio-orthogonal vibrations	+++	++	+++	++	Quantitative	Subcellular (300 nm)